Journal of Computational Physics 228 (2009) 1678–1712

Contents lists available at ScienceDirect

Journal of Computational Physics

journal homepage: www.elsevier.com/locate/jcp

Simple and efficient relaxation methods for interfaces separating compressible fluids, cavitating flows and shocks in multiphase mixtures

Richard Saurel [a,b,*], Fabien Petitpas [a], Ray A. Berry [c]

[a] Polytech'Marseille, Aix-Marseille University and SMASH Project UMR CNRS 6595 – IUSTI-INRIA, 5 rue E. Fermi, 13453 Marseille Cedex 13, France
[b] University Institute of France and SMASH Project UMR CNRS 6595 – IUSTI-INRIA, 5 rue E. Fermi, 13453 Marseille Cedex 13, France
[c] Multiphysics Methods Group, Advanced Nuclear Energy Systems Department, Idaho National Laboratory, P.O. Box 1625, Idaho Falls, ID 83415-3885, United States

ARTICLE INFO

Article history:
Received 16 April 2008
Received in revised form 13 October 2008
Accepted 3 November 2008
Available online 13 November 2008

Keywords:
Hyperbolic systems
Multifluid
Multiphase
Real gases
Cavitation
Multiphysic
Godunov

ABSTRACT

Numerical approximation of the five-equation two-phase flow of Kapila et al. [A.K. Kapila, R. Menikoff, J.B. Bdzil, S.F. Son, D.S. Stewart, Two-phase modeling of deflagration-to-detonation transition in granular materials: reduced equations, Physics of Fluids 13(10) (2001) 3002–3024] is examined. This model has shown excellent capabilities for the numerical resolution of interfaces separating compressible fluids as well as wave propagation in compressible mixtures [A. Murrone, H. Guillard, A five equation reduced model for compressible two phase flow problems, Journal of Computational Physics 202(2) (2005) 664–698; R. Abgrall, V. Perrier, Asymptotic expansion of a multiscale numerical scheme for compressible multiphase flows, SIAM Journal of Multiscale and Modeling and Simulation (5) (2006) 84–115; F. Petitpas, E. Franquet, R. Saurel, O. Le Metayer, A relaxation-projection method for compressible flows. Part II. The artificial heat exchange for multiphase shocks, Journal of Computational Physics 225(2) (2007) 2214–2248]. However, its numerical approximation poses some serious difficulties. Among them, the non-monotonic behavior of the sound speed causes inaccuracies in wave's transmission across interfaces. Moreover, volume fraction variation across acoustic waves results in difficulties for the Riemann problem resolution, and in particular for the derivation of approximate solvers. Volume fraction positivity in the presence of shocks or strong expansion waves is another issue resulting in lack of robustness. To circumvent these difficulties, the pressure equilibrium assumption is relaxed and a pressure non-equilibrium model is developed. It results in a single velocity, non-conservative hyperbolic model with two energy equations involving relaxation terms. It fulfills the equation of state and energy conservation on both sides of interfaces and guarantees correct transmission of shocks across them. This formulation considerably simplifies numerical resolution. Following a strategy developed previously for another flow model [R. Saurel, R. Abgrall, A multiphase Godunov method for multifluid and multiphase flows, Journal of Computational Physics 150 (1999) 425–467], the hyperbolic part is first solved without relaxation terms with a simple, fast and robust algorithm, valid for unstructured meshes. Second, stiff relaxation terms are solved with a Newton method that also guarantees positivity and robustness. The algorithm and model are compared to exact solutions of the Euler equations as well as solutions of the five-equation model under extreme flow conditions, for interface computation and cavitating flows involving dynamics appearance of interfaces. In order to deal with correct dynamic of shock waves propagating through multiphase mixtures, the artificial heat exchange method of Petitpas et al. [F. Petitpas, E. Franquet, R. Saurel, O. Le Metayer, A relaxation-projection method for

* Corresponding author. Address: Polytech'Marseille, Aix-Marseille University and SMASH Project UMR CNRS 6595 – IUSTI-INRIA, 5 rue E. Fermi, 13453 Marseille Cedex 13, France. Tel.: +33 339 128 8511; fax: +33 339 128 8322.
E-mail address: Richard.Saurel@polytech.univ-mrs.fr (R. Saurel).

0021-9991/$ - see front matter
doi:10.1016/j.jcp.2008.11.002

compressible flows. Part II. The artificial heat exchange for multiphase shocks, Journal of Computational Physics 225(2) (2007) 2214–2248] is adapted to the present formulation.

1. Introduction

Compressible multi-material flows and multiphase mixtures arise in many natural and industrial situations including bubble dynamics, shock wave interaction with material discontinuities, detonation of high energetic materials, hypervelocity impacts, cavitating flows, combustion systems to name only a few. The motivation of the present work is the accurate and computationally efficient resolution of interface problems in extreme flow conditions (high pressure ratios $\approx 10^7$, high density ratios $\approx 10^3$), as well as the computation of dynamic appearance of interfaces, that occur in cavitating flows and spallation phenomena. These interfaces are often separating pure media but also mixtures of materials in which wave dynamics is also important. Such situations appear frequently in astrophysics, physics of explosives, nuclear physics, powder engineering and many other applications. The aim of the present paper is to develop a general formulation and algorithm to solve interface problems separating compressible media or mixtures in extreme situations.

Godunov type schemes and variants have now reached a level of maturity to solve single phase flows in the presence of discontinuities. However, the presence of large discontinuities of thermodynamic variables and equations of state at material interfaces result in numerical instabilities, oscillations and computational failure [24,1].

To circumvent these difficulties, two classes of methods have been developed:

- Methods that consider the interface as a sharp discontinuity (Sharp Interface Methods – SIM).
- Methods that consider the interface as a diffuse zone, like contact discontinuities in gas dynamics (Diffuse Interface Methods – DIM).

The Lagrangian class of SIM is the most natural (see for example [21,14]). In this context, the computational mesh moves and distorts with the material interface. However, when dealing with fluid flows, deformations are unbounded and resulting mesh distortions can make the Lagrangian approach unpractical [46]. Eulerian methods use a fixed mesh with an additional equation for tracking or reconstructing the material interface. In the volume of fluid (VOF) approach [20], each computational cell is assumed to possibly contain a mixture of both fluids and the volume occupied by each fluid is represented by the volume fraction, transported with the flow. This method is widely used for incompressible flows as there is no special thermodynamics to compute in mixture cells [19]. For compressible flows, extra energy equations are used as well as pressure relaxation procedures [7,32]. These methods seem efficient as a result of subtle management at the discrete level of the various equations. The literature does not provide a clear link of this discrete management to a given system of continuous partial differential equations. In the present paper an attempt to clarify, improve and generalize these methods will be developed.

Another class of popular Eulerian methods is based on the level-set equation [13,34,36,47] to locate the interface. Again, for compressible flows, special management of the interface is needed to guarantee interface conditions. Relevant work in this direction was done by Fedkiw et al. [16] with the Ghost Fluid Method, Abgrall and Karni [2] with a simplified version of this method and Khoo et al. [25]. This method is attractive for its apparent simplicity and versatility versus various problems of physics. However, its use in arbitrary conditions, with large pressure and density ratios does not seem obvious. Moreover, it is non-conservative regarding mixture variables (momentum and energy). The last class of SIM corresponds to Front Tracking methods where the interface is explicitly tracked over a fixed Eulerian mesh. Considerable efforts have been done to develop computational codes employing this approach [18,30].

It is worth mentioning that none of these methods is able to dynamically create interfaces and to solve interfaces separating pure media and mixtures.

The second type of methods (DIM) considers interfaces as numerically diffused zones, like contact discontinuities in gas dynamics. Diffuse interfaces correspond to artificial mixtures created by numerical diffusion. A pioneering work in this direction was performed by Abgrall [1]. Determination of thermodynamic flow variables in these zones is achieved on the basis of multiphase flow theory ([40,4,42,35,3,43,37]). The challenge is to derive physically, mathematically, and numerically consistent thermodynamic laws for the artificial mixture. The key issue is to fulfill interface conditions within this artificial mixture. This second category possesses several advantages:

- The same algorithm is implemented globally in both pure fluids and in mixture zones. An extended hyperbolic system is used to solve every location of the flow.
- These models and methods are able to dynamically create interfaces that are not present initially, e.g. in cavitating flows where gas pockets dynamically appear in a liquid [41,29,45].
- These methods are also able to deal with interfaces separating pure fluids and fluid mixtures, e.g. in the computation of detonation waves in condensed explosives where chemical decomposition produces multiphase mixtures of materials [41,8,38].

Methods in this second category are based on hyperbolic multiphase flow models, consisting of two main classes:

- Models for mixtures in total non-equilibrium: Baer and Nunziato [5] model and its variants, and
- Models for mixtures in mechanical equilibrium [49,23].

This paper deals with the building of a simple, robust, fast and accurate formulation for single velocity and single pressure multiphase flows. The Kapila et al. [23] model is of particular interest for the computation of interfaces separating compressible fluids, as well as barotropic and non-barotropic cavitating flows. Specific numerical schemes have been derived recently in Murrone and Guillard [35], Abgrall and Perrier [3], Saurel et al. [43], Petitpas et al. [37].

This model is apparently simple. In the context of two fluids it is composed of two mass equations, a mixture momentum equation and a mixture energy equation. These equations express in conservative formulation. The closure is achieved by the pressure equilibrium condition that results in a differential transport equation for the volume fraction containing a non-conservative term, involving the velocity divergence and phasic bulk modulii. However this last equation poses serious computational challenges which include:

- Shock computations within the context of a non-conservative model.
- Volume fraction positivity, when dealing with shocks and strong expansion waves. The term involving a velocity divergence in the volume fraction evolution equation is particularly difficult to approximate [37]. This is particularly important for the dynamic appearance of interfaces in cavitating flows.
- Non-monotonic behavior of the sound speed [54] resulting in inaccurate wave transmission across diffuse interfaces. In the diffuse interface the sound speed presents large variations resulting in wrong acoustic wave dynamics. The wave's chronology is thus in error, as will be shown in more details in the next paragraph.

Moreover, in order to consider future extensions with additional physics to reach multiphysics modeling of continuous media with a multiphase approach, the computational efficiency of existing algorithms must be improved. The multiphysics challenge we consider deals with:

- Sophisticated equations of state (EOS): Mie-Gruneisen for condensed materials, JWL for explosive products [28], etc.
- Granular materials that involve extra EOS expressing contact granular energy and contact pressure [6].
- Capillary effects modeling [39] with eventually phase transition [45].
- Interfaces separating compressible fluids and elastic solids in extreme deformations [33,50,17,15]. This instance is particularly difficult as the EOS for solids depends on the deformation tensor.

The present paper does not deal with all these extensions, but it is clear that such a goal needs simple and robust multiphase formulations. The present paper addresses this issue in the context of the simplest version of the Kapila et al. [23] model.

The main difficulty with this model comes from the pressure equilibrium condition, which results in the non-conservative equation for the volume fraction. A conservative formulation can be obtained with the help of the entropy equations. However, this conservative formulation is untenable in the presence of shocks.

To circumvent these difficulties, pressure non-equilibrium effects are restored in the Kapila et al. [23] model. This results in a 6-equation model with a single velocity but with two pressures and associated relaxation terms. This extended model was already presented as a first reduction of the Baer and Nunziato [5] model in [23], but never considered for the description of diffuse interfaces. A seventh equation is added describing the mixture total energy in order to guarantee a correct treatment of shocks in the single phase limit. This apparent complexity with an extended model actually leads to considerable simplifications regarding numerical resolution. Indeed, this model remains hyperbolic with only three characteristic wave propagation speeds and volume fraction positivity is easily preserved. The building of a simple and efficient method for the numerical approximation of this flow model in the context of diffuse interfaces is the aim of the present paper.

When relaxation terms are omitted the volume fraction remains constant across acoustic waves and the Riemann problem is easily solved with approximate Riemann solvers (acoustic and HLLC-type solvers, [52]). Moreover, the building of a positivity preserving scheme guarantees robustness when considering cavitating flows [26,48,37] where interfaces appear dynamically. Dynamic appearance of these interfaces is a consequence of pressure relaxation, done at the end of each hyperbolic evolution step, in order to match asymptotically solutions of the Kapila et al. [23] reduced model.

This paper is organized as follows. In Section 2 the Kapila et al. [23] model is recalled and the non-equilibrium 6-equation model is presented. This 6-equation model tends to the 5-equation model of Kapila et al. [23] in the limit of stiff pressure relaxation. Basic properties of these models are presented: Entropy inequality and hyperbolicity. In Section 3 the numerical method is built. Approximate Riemann solvers are presented for the hyperbolic part and a Godunov type scheme is built. The pressure relaxation algorithm is also presented in this Section. Special attention is given to the role of the seventh equation used to correct the computation of non-conservative energies in the single phase limit, on both sides of an interface. Various test cases are presented in Section 4, together with validations against exact solutions of the Euler equations and of the 5-equation model of Kapila et al. [23]. Some examples consider interfaces initially present in the flow, while others involve the dynamic appearance of interfaces. Section 5 presents the extension of the method to shock propagation in physical

multiphase mixtures. This extension is not important for interfaces separating pure (or nearly pure) fluids. But it has importance when the interface separates pure fluids and mixtures of materials. Finally, conclusions and future investigations are discussed in Section 6.

Difficulties are often reported to solve barotropic cavitating flow models. The present method being general, it can also be applied to this type of model. Thus, comparisons of the 6-equation model have been added with existing barotropic cavitating flow models [53] in Appendix A. These models are recovered as limiting cases of the present 6-equation model. Moreover, a simple algorithm is proposed to solve cavitating barotropic flows.

2. Pressure equilibrium and non-equilibrium single velocity multiphase flow models

The single velocity pressure equilibrium model corresponds to the one of Kapila et al. [23]. It has been obtained as the asymptotic limit of the Baer and Nunziato [5] model in the limit of both stiff velocity and pressure relaxation. It involves 5 partial differential equations, one of them being non-conservative. Its resulting speed of sound corresponds to that of [54] which exhibits a non-monotonic variation with volume fraction. These two difficulties (non-conservativity and non-monotonicity) present serious computational challenges. To circumvent them, a pressure non-equilibrium 6-equation model is constructed (first reduced model in [23]), also non-conservative but easier to solve with a relaxation method. Both models are presented hereafter.

2.1. Five-equation model

The Kapila et al. [23] is the zero-order approximation of the Baer and Nunziato [5] with stiff mechanical relaxation. It reads in the context of two fluids:

$$\begin{aligned}
&\frac{\partial \alpha_1}{\partial t} + u\frac{\partial \alpha_1}{\partial x} = \frac{\rho_2 c_2^2 - \rho_1 c_1^2}{\frac{\rho_1 c_1^2}{\alpha_1} + \frac{\rho_2 c_2^2}{\alpha_2}} \frac{\partial u}{\partial x},\\
&\frac{\partial (\alpha\rho)_1}{\partial t} + \frac{\partial (\alpha\rho)_1 u}{\partial x} = 0,\\
&\frac{\partial (\alpha\rho)_2}{\partial t} + \frac{\partial (\alpha\rho)_2 u}{\partial x} = 0,\\
&\frac{\partial \rho u}{\partial t} + \frac{\partial \rho u^2 + p}{\partial x} = 0,\\
&\frac{\partial \rho E}{\partial t} + \frac{\partial (\rho E + p) u}{\partial x} = 0,
\end{aligned} \tag{II.1}$$

where α, ρ, u, p, E ($E = e + \frac{1}{2}u^2$), and e represent respectively the volume fraction, the mixture density, the velocity, the mixture pressure, the mixture total energy and the mixture internal energy.

The mixture internal energy is defined as

$$e = Y_1 e_1(\rho_1, p) + Y_2 e_2(\rho_2, p) \tag{II.2}$$

and the mass fraction is given by: $Y_k = \frac{(\alpha\rho)_k}{\rho}$.

The mixture density is defined by $\rho = (\alpha\rho)_1 + (\alpha\rho)_2$.

Each fluid is governed by its own convex equation of state (EOS),

$$e_k = e_k(\rho_k, p),$$

which allows the determination of the phases' sound speed,

$$c_k = c_k(\rho_k, p).$$

The mixture pressure p is determined by solving Eq. (II.2). In the particular case of fluids governed by the stiffened gas EOS,

$$p_k = (\gamma_k - 1)\rho_k e_k - \gamma_k p_{\infty k}, \tag{II.3}$$

the resulting mixture EOS reads,

$$p(\rho, e, \alpha_1, \alpha_2) = \frac{\rho e - \left(\frac{\alpha_1 \gamma_1 p_{\infty 1}}{\gamma_1 - 1} + \frac{\alpha_2 \gamma_2 p_{\infty 2}}{\gamma_2 - 1}\right)}{\frac{\alpha_1}{\gamma_1 - 1} + \frac{\alpha_2}{\gamma_2 - 1}} \tag{II.4}$$

It is straightforward to obtain the entropy equations:

$$\frac{ds_k}{dt} = 0, \quad k = 1, 2.$$

Consequently, this model needs specific relations for its closure in the presence of shocks. In the limit of weak shocks, appropriate shock relations have been determined in [44]:

$$\begin{aligned} &Y_k = Y_k^0, \\ &\rho(u-\sigma) = \rho^0(u^0-\sigma) = m, \\ &p - p^0 + m^2(v - v^0) = 0, \\ &e_k - e_k^0 + \frac{p+p^0}{2}(v_k - v_k^0) = 0, \end{aligned} \tag{II.5}$$

where σ denotes the shock speed and the upperscript '0' represents the unshocked state.

These relations have been intensively validated against a large experimental data base for *weak and strong shocks* in the same reference.

Even equipped with these relations, this apparently simple model involves many difficulties:

- With the help of relations (II.5), it is possible to solve exactly or approximately the Riemann problem [37]. Even when this solution is exact, it is shown in the same reference that convergence of a numerical scheme to the exact solution is extremely difficult as the system is non-conservative: The cell average of non-conservative variables has no physical sense. Cell averages were replaced by a relaxation procedure in [43,37]. To reach convergence for shock propagating in multiphase mixtures, artificial heat exchanges were needed in the shock layer [37].
- Another issue is related to the volume fraction positivity in the presence of shocks and even in the presence of strong rarefaction waves. Indeed, when dealing with liquid–gas mixtures for example, the liquid compressibility is so weak that the pressure tends to become negative, resulting in computational failure in the gas sound speed computation. Such situation occurs frequently in cavitation test problems.
- An extra difficulty is related to the mixture sound speed that obeys the Wood [54] formula $\frac{1}{\rho c_{eq}^2} = \frac{\alpha_1}{\rho_1 c_1^2} + \frac{\alpha_2}{\rho_2 c_2^2}$. The mixture sound speed has a non-monotonic variation with volume fraction, as shown in Fig. 1. Here c_{eq} represents the mechanical equilibrium mixture sound speed.

To illustrate the difficulties related to the non-monotonic sound speed in this model, numerical results obtained with the method of Petitpas et al. [37] are recalled. This method solves interfaces as diffuse numerical zones with the help of a Lagrange-relaxation algorithm. A 1-m long shock tube containing two chambers separated by an interface at the location $x = 0.8$ m is considered. Each chamber contains a mixture of water and air. The initial density of the water is $\rho_{water} = 1000\ kg\ m^{-3}$ and the stiffened gas EOS parameters are $\gamma_{water} = 4.4$ and $p_{\infty,water} = 6 \times 10^8$ Pa. The initial density of air is $\rho_{air} = 10\ kg\ m^{-3}$ and EOS parameters are $\gamma_{air} = 1.4$ and $p_{\infty,air} = 0$ Pa. The left chamber contains a very small volume fraction of air $\alpha_{air} = 10^{-6}$ and the pressure is equal to 10^9 Pa. The right chamber contains the same fluids but the volume fractions are reversed. Its pressure is equal to 10^5 Pa. In both chambers the initial velocity is zero. The exact solution of the single phase Euler equations and the multiphase flow model with five equations are compared in Fig. 2 at time $t = 220$ μs.

A bad consequence of the Wood [54] speed of sound appears when a pressure wave interacts with a diffuse interface. To illustrate this difficulty, let us consider the advection of a water–air interface at the velocity of 50 m/s. The numerical solution of this advection test with a first-order accuracy method is shown in Fig. 3 where the behaviors of the equilibrium speed of sound [54] and another mixture sound speed (frozen) are compared. The frozen speed of sound is defined by $c_f^2 = Y_{water} c_{water}^2 + Y_{air} c_{air}^2$ and will appear as a major feature of the non-equilibrium 6-equation model.

It is clear that the use of the equilibrium speed of sound creates a zone where the speed of sound is lower than those of the two initial media. This may have serious consequences regarding wave's propagation. To illustrate the difficulty let us consider the interaction of an acoustic wave with this diffused interface. When a wave propagates through the interface,

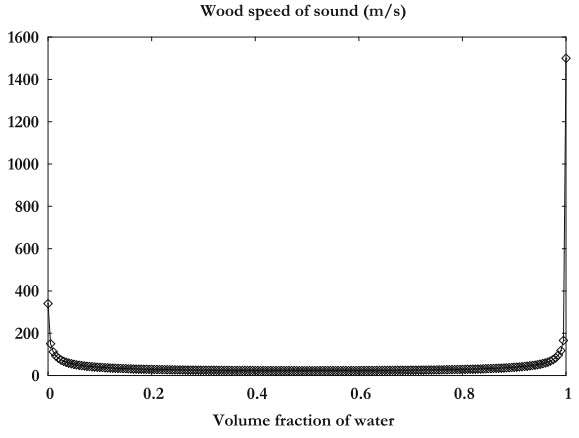

Fig. 1. Representation of the mixture equilibrium speed of sound ($1/\rho c_{eq}^2 = \alpha_1/\rho_1 c_1^2 + \alpha_2/\rho_2 c_2^2$) of the 5-equation model for the liquid water–air mixture under atmospheric conditions.

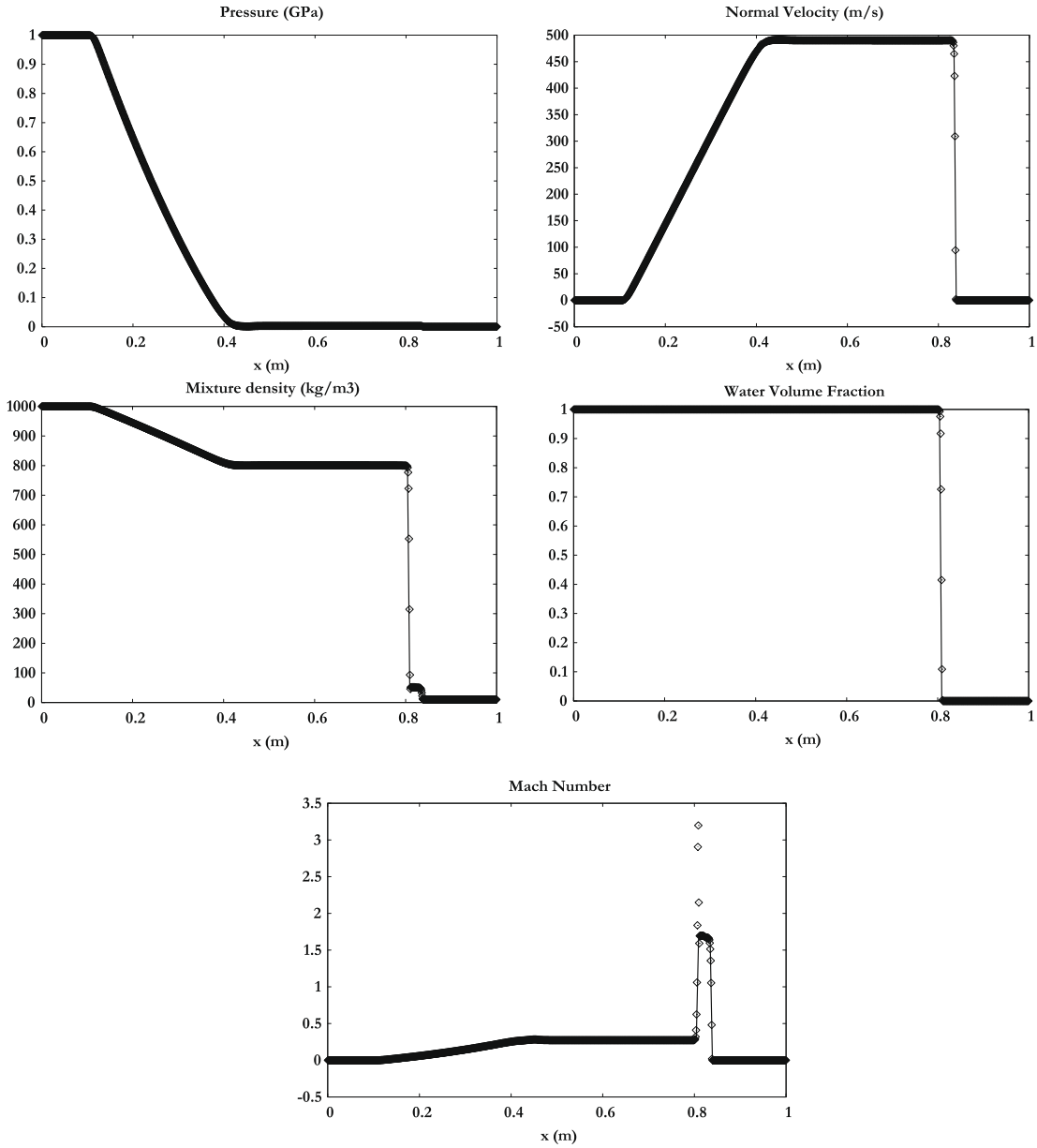

Fig. 2. Liquid/gas shock tube. The Lagrange-relaxation method (symbols) of Petitpas et al. [37] is compared to the exact solution (solid). A 1000 cells mesh is used. The density ratio is 100 and the pressure ratio is 10,000 at the initial discontinuity. A Mach oscillation appears in the numerical diffusion zone at the interface and is due to the non-monotonic behavior of the speed of sound of this model.

it crosses a first zone with stiff variation of the sound speed, possibly resulting in partial diffraction. The transmitted wave propagates in the numerical diffusion zone with very low velocity before reaching the second stiff variation of sound speed, resulting in a second diffraction. These various effects (multiple diffractions) and low sound speed induce delay for the wave's transmission (Fig. 4).

The method developed in the present paper is aimed to improve accuracy, robustness and computational efficiency of existing methods for the Kapila et al. [23] model regarding:

- Volume fraction positivity. This is a particularly difficult issue when dealing with dynamic appearance of interfaces in nearly pure liquids and solids.
- Computation of cavitating flows. These flows involve extra difficulties related to the drastic Mach number evolutions ranging from 0.01 to 100 [26,11,48]. These references report this problem in the simpler context of a cavitation model in conservative form that will be examined in Appendix A.
- Riemann problem resolution, that is quite difficult to solve with the Wood [54] sound speed.

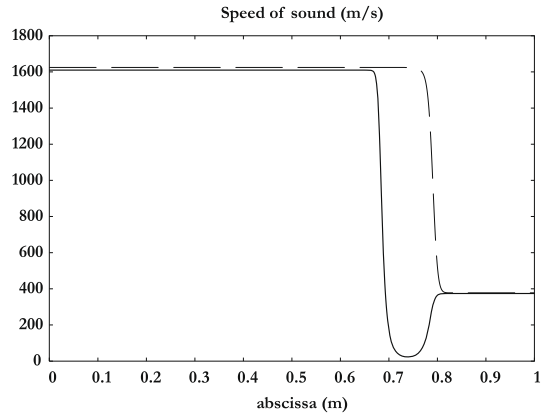

Fig. 3. Comparison of equilibrium (lines) and frozen (dashed lines) speed of sound during numerical advection of a water–air interface. In the numerical diffusion zone at the interface the equilibrium speed of sound is lower than in pure fluids. This may have serious consequences on wave transmission (in particular regarding chronology) when a pressure wave interacts with this diffused zone.

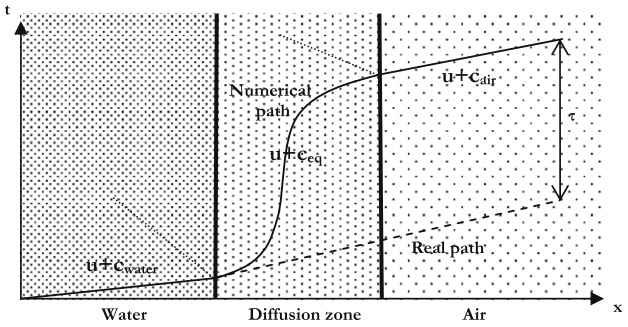

Fig. 4. Schematic representation in the (x, t) diagram of the interaction between an acoustic wave and the numerical diffusion zone of an interface computed with the equilibrium speed of sound [54]. In the numerical diffusion zone, the transmitted wave propagates at a lower velocity than in the pure fluids. This induces a delay τ in the wave's transmission through the interface.

- Wave transmission through diffuse interfaces, as presented in Fig. 4.
- Computations on unstructured meshes. Not all existing methods for the Kapila et al. [23] model are able to deal with unstructured meshes.

A pressure non-equilibrium model is considered in these aims.

2.2. Six-equation model

The 6-equation model is also derived from the 7-equation model of Baer and Nunziato [5] in the asymptotic limit of stiff velocity relaxation only (first reduced model in [23]). Pressure non-equilibrium effects are maintained. The 6-equation model should not be considered as a physical model, but more as a step-model to solve the 5-equations model (second reduced model of [23]). Indeed, the model with 6-equations has better properties for numerical approximations than the mechanical equilibrium one:

- Positivity of the volume fraction is easily preserved.
- The mixture sound speed has a monotonic behavior which seems to be more attractive regarding diffused interfaces and acoustic wave transmission.

These two properties are key points for the building of a simple, robust and accurate hyperbolic solver. Moreover, with proper treatment of relaxation terms, solutions of the 5-equation model will be recovered.

2.2.1. Flow model

The 6-equation model reads:

$$\frac{\partial \alpha_1}{\partial t} + u\frac{\partial \alpha_1}{\partial x} = \mu(p_1 - p_2),$$

$$\begin{aligned}
&\frac{\partial \alpha_1\rho_1}{\partial t}+\frac{\partial \alpha_1\rho_1 u}{\partial x}=0,\\
&\frac{\partial \alpha_2\rho_2}{\partial t}+\frac{\partial \alpha_2\rho_2 u}{\partial x}=0,\\
&\frac{\partial \rho u}{\partial t}+\frac{\partial \rho u^2+(\alpha_1 p_1+\alpha_2 p_2)}{\partial x}=0,\\
&\frac{\partial \alpha_1\rho_1 e_1}{\partial t}+\frac{\partial \alpha_1\rho_1 e_1 u}{\partial t}+\alpha_1 p_1\frac{\partial u}{\partial x}=-p_I\mu(p_1-p_2),\\
&\frac{\partial \alpha_2\rho_2 e_2}{\partial t}+\frac{\partial \alpha_2\rho_2 e_2 u}{\partial t}+\alpha_2 p_2\frac{\partial u}{\partial x}=p_I\mu(p_1-p_2).
\end{aligned} \tag{II.6}$$

The interfacial pressure p_I is obtained as the asymptotic limit of the interfacial pressure of the symmetric non-equilibrium model with 7-equations of Saurel et al. [42]. This estimate in the limit of equal velocities reads:

$$p_I=\frac{Z_2p_1+Z_1p_2}{Z_1+Z_2},$$

where $Z_k=\rho_k c_k$ represents the acoustic impedance of phase k.

The combination of the two internal energy equations with mass and momentum equations results in the additional mixture energy equation:

$$\frac{\partial \rho(Y_1e_1+Y_2e_2+\frac{1}{2}u^2)}{\partial t}+\frac{\partial u\big(\rho(Y_1e_1+Y_2e_2+\frac{1}{2}u^2)+(\alpha_1p_1+\alpha_2p_2)\big)}{\partial x}=0. \tag{II.7}$$

This extra equation will be important during numerical resolution, in order to correct inaccuracies due to the numerical approximation of the two non-conservative internal energy equations in the presence of shocks.

There is no difficulty to check that the second law of thermodynamics is fulfilled by this model. The phasic entropy equations are readily obtained:

$$\begin{aligned}
&\alpha_1\rho_1T_1\frac{ds_1}{dt}=\mu(p_1-p_2)^2\frac{Z_1}{Z_1+Z_2},\\
&\alpha_2\rho_2T_2\frac{ds_2}{dt}=\mu(p_1-p_2)^2\frac{Z_2}{Z_1+Z_2},
\end{aligned}$$

insuring that the mixture entropy ($s=Y_1s_1+Y_2s_2$) always evolve with positive or null variations.

This model exhibits a nice feature with respect to the mixture sound speed. The mixture sound speed,

$$c_f^2=Y_1c_1^2+Y_2c_2^2,$$

has a monotonic behavior versus volume and mass fractions and represents the frozen mixture sound speed.

The model is thus strictly hyperbolic with waves speeds: $u+c_f$, $u-c_f$, u. A more detailed analysis of hyperbolicity and sound speed will be carried out in Section 3 with the approximate acoustic Riemann solver.

2.2.2. About shock relations

As with the previous 5-equation model, the new model is also non-conservative, and shock relations have to be prescribed. However, the preceding remarks about shock relations for the five equations model and numerical approximation of shocks with non-conservative systems yield the following conclusion:

Even when shock relations are known or accepted for a non-conservative system, it is very difficult to make the numerical solution converge to the end shock state solution.

There is thus no need to determine precise shock relations for the 6-equation model, in particular since it is intended only to approximate the 5-equation model for which shock relations are known.

However, some admissibility conditions have to be respected by a given Hugoniot approximate model. Jump conditions must at least respect [44]:

- Energy conservation of the mixture.
- Tangency of the mixture Hugoniot curve and mixture isentrope.
- Single phase limit for which jump conditions are unambiguously known.
- Symmetry.
- Entropy production.

Jump conditions for the mass equations are

$$\begin{aligned}
&\alpha_1\rho_1(u-\sigma)=\alpha_1^0\rho_1^0(u^0-\sigma)=m_1,\\
&\alpha_2\rho_2(u-\sigma)=\alpha_2^0\rho_2^0(u^0-\sigma)=m_2.
\end{aligned}$$

Let us denote the mixture pressure by $p = \alpha_1 p_1 + \alpha_2 p_2$ and the shock mass flow rate by $m = m_1 + m_2$. With these notations, the momentum jump condition can be written

$$p - p^0 + m^2(v - v^0) = 0.$$

The mixture energy jump condition is:

$$e - e^0 + \frac{p + p^0}{2}(v - v^0) = 0,$$

with $e = Y_1 e_1 + Y_2 e_2$ and $v = Y_1 v_1 + Y_2 v_2$ ($v_k = \frac{1}{\rho_k}$).

In the absence of relaxation effects the volume fraction jump is simply:

$$\alpha_1 = \alpha_1^0.$$

The non-conservative internal energy equations are not adapted to the determination of jump conditions. Following the preceding admissibility conditions the following jump conditions are proposed:

$$e_k - e_k^0 + \frac{p_k + p_k^0}{2}(v_k - v_k^0) = 0. \tag{II.8}$$

The conditions that must be satisfied include:

- *Energy conservation*

The sum of the internal energy jump equations yields:

$$Y_1(e_1 - e_1^0) + \frac{p_1 + p_1^0}{2}(Y_1 v_1 - Y_1 v_1^0) + Y_2(e_2 - e_2^0) + \frac{p_2 + p_2^0}{2}(Y_2 v_2 - Y_2 v_2^0) = 0.$$

As $Y_k = \frac{\alpha_k v}{v_k}$, we have:

$$e - e^0 + \frac{p_1 + p_1^0}{2}(\alpha_1 v - \alpha_1^0 v^0) + \frac{p_2 + p_2^0}{2}(\alpha_2 v - \alpha_2^0 v^0) = 0.$$

With the volume fraction jump relation, this equation becomes

$$e - e^0 + \frac{\alpha_1 p_1 + \alpha_2 p_2 + \alpha_1 p_1^0 + \alpha_2 p_2^0}{2}(v - v^0) = 0,$$

or simply

$$e - e^0 + \frac{p + p^0}{2}(v - v^0) = 0.$$

This result guarantees that the phasic energy jump conditions are compatible with the mixture energy conservation.

- *Tangency of the mixture Hugoniot curve and isentrope*

This is a mandatory property for the Riemann problem solution. As the volume fraction is constant across shocks and rarefaction waves (in absence of relaxation effects) and the phasic Hugoniots are tangent to phasic isentropes, the mixture Hugoniot is necessarily tangent to the mixture isentrope.

- *Single phase limit*

When one of the phases disappears the energy jump condition of the remaining fluid is in agreement with the single phase energy jump.

- *Symmetry*

Symmetry in the formulation allows an easy extension to an arbitrary number of fluids.

- *Entropy production*

As each phase evolves along its own Hugoniot (II.8) there is no doubt that the mixture entropy evolves positively.

Through application of these relations, the Riemann problem can now be solved. Numerical issues pertaining to the Riemann problem solution are addressed in the next section. Let us insist on the fact that jump conditions are not the key to shock computation in multiphase mixtures. It has been shown that even when shock relations are known, the convergence of a numerical scheme to the exact solution is very difficult. This is due to the lack of definition for cell averages of non-conservative variables [37].

2.2.3. Asymptotic limit

As the method will solve the 6-equation model with stiff relaxation terms, it is important to check that in the limit of infinitely fast pressure relaxation the 5-equation model is recovered. This proof is given in Appendix B.

3. Numerical method

Numerical resolution of the 6-equation model in the limit of stiff pressure relaxation is addressed in the present section. In regular zones, this model is self consistent. But in the presence of shocks the internal energy equations are inappropriate. To correct the thermodynamic state predicted by these equations in the presence of shocks, the total mixture energy equation will be used. This correction will be valid on both sides of an interface, when the flow tends to the single phase limits. The details of this correction will be examined further. For now, the 6-equation system is augmented by a redundant equation regarding the total mixture energy. The system to consider during numerical resolution thus involves seven equations:

$$\begin{aligned}
&\frac{\partial \alpha_1}{\partial t} + u\frac{\partial \alpha_1}{\partial x} = \mu(p_1 - p_2),\\
&\frac{\partial \alpha_1\rho_1 e_1}{\partial t} + \frac{\partial \alpha_1\rho_1 e_1 u}{\partial x} + \alpha_1 p_1 \frac{\partial u}{\partial x} = -p_I\mu(p_1 - p_2),\\
&\frac{\partial \alpha_2\rho_2 e_2}{\partial t} + \frac{\partial \alpha_2\rho_2 e_2 u}{\partial x} + \alpha_2 p_2 \frac{\partial u}{\partial x} = p_I\mu(p_1 - p_2),\\
&\frac{\partial \alpha_1\rho_1}{\partial t} + \frac{\partial \alpha_1\rho_1 u}{\partial x} = 0,\\
&\frac{\partial \alpha_2\rho_2}{\partial t} + \frac{\partial \alpha_2\rho_2 u}{\partial x} = 0,\\
&\frac{\partial \rho u}{\partial t} + \frac{\partial \rho u^2 + (\alpha_1 p_1 + \alpha_2 p_2)}{\partial x} = 0,\\
&\frac{\partial \rho(Y_1 e_1 + Y_2 e_2 + \frac{1}{2}u^2)}{\partial t} + \frac{\partial u\big(\rho(Y_1 e_1 + Y_2 e_2 + \frac{1}{2}u^2) + (\alpha_1 p_1 + \alpha_2 p_2)\big)}{\partial x} = 0
\end{aligned} \tag{III.1}$$

with $p_I = \frac{Z_2 p_1 + Z_1 p_2}{Z_1 + Z_2}$ and appropriate equations of state $e_k = e_k(\rho_k, p_k)$.

This system is equipped with the approximate shock relations of the preceding section, in particular relation (II.8).

3.1. Approximate Riemann solvers

Two types of approximate Riemann solvers will be considered:

- Acoustic linearized Riemann solver,
- HLLC Riemann solver.

These two solvers are detailed in the context of the Euler equations in Toro [52].

3.1.1. Acoustic solver

This approximate solver assumes that shocks are absent or sufficiently weak. The last equation of system (III.1) can thus be suppressed. Indeed, this last equation is only used to correct some deficiencies of the numerical resolution of phase's internal energy equations in the presence of shocks. The 6-equation system free of relaxation terms can thus be written with the following variables:

$$\frac{\partial W}{\partial t} + A(W)\frac{\partial W}{\partial x} = 0,$$

with $W = (\alpha_1, s_1, s_2, u, p_1, p_2)^{\mathrm{T}}$ and,

$$A(W) = \begin{pmatrix} u & 0 & 0 & 0 & 0 & 0\\ 0 & u & 0 & 0 & 0 & 0\\ 0 & 0 & u & 0 & 0 & 0\\ \frac{p_1 - p_2}{\rho} & 0 & 0 & u & \frac{\alpha_1}{\rho} & \frac{\alpha_2}{\rho}\\ 0 & 0 & 0 & \rho_1 c_1^2 & u & 0\\ 0 & 0 & 0 & \rho_2 c_2^2 & 0 & u \end{pmatrix}.$$

Eigenvalues of the propagation matrix are:

$\lambda_0 = u$, four times fold, $\lambda_1 = u - c$, $\lambda_2 = u + c$, with,

$$c^2 = Y_1 c_1^2 + Y_2 c_2^2 \tag{III.2}$$

The frozen sound speed introduced in Section 2 is now established.

The acoustic solver is based on characteristic equations that are readily obtained:

- Along trajectories defined by $\frac{dx}{dt} = u$

$$\frac{d\alpha_1}{dt} = 0, \quad \frac{ds_1}{dt} = 0, \quad \frac{ds_2}{dt} = 0.$$

- Along trajectories defined by $\frac{dx}{dt} = u - c$

$$-\frac{p_1 - p_2}{\rho c}\frac{d\alpha_1}{dt}\Big)_{u-c} + \frac{du}{dt}\Big)_{u-c} - \frac{\alpha_1}{\rho c}\frac{dp_1}{dt}\Big)_{u-c} - \frac{\alpha_2}{\rho c}\frac{dp_2}{dt}\Big)_{u-c} = 0$$

- Along trajectories defined by $\frac{dx}{dt} = u + c$

$$\frac{p_1 - p_2}{\rho c}\frac{d\alpha_1}{dt}\Big)_{u+c} + \frac{du}{dt}\Big)_{u+c} + \frac{\alpha_1}{\rho c}\frac{dp_1}{dt}\Big)_{u+c} + \frac{\alpha_2}{\rho c}\frac{dp_2}{dt}\Big)_{u+c} = 0.$$

These relations are used to solve the linearized Riemann problem. By assuming weak variations across left- and right-facing waves, the acoustic impedance $Z = \rho c$ (with c defined by (III.2) and ρ the mixture density) are assumed constant. The corresponding jump relations are:

- Across a right-facing wave,

$$\alpha_{1R}^* = \alpha_{1R}, s_{1R}^* = s_{1R}, \; s_{2R}^* = s_{2R},$$
$$(\alpha_1 p_1 + \alpha_2 p_2)_R^* - Z_R u_R^* = (\alpha_1 p_1 + \alpha_2 p_2)_R - Z_R u_R \quad \text{with } Z_R = \rho_R c_R.$$

- Across a left-facing wave,

$$\alpha_{1L}^* = \alpha_{1L}, \; s_{1L}^* = s_{1L}, \; s_{2L}^* = s_{2L},$$
$$(\alpha_1 p_1 + \alpha_2 p_2)_L^* + Z_L u_L^* = (\alpha_1 p_1 + \alpha_2 p_2)_L + Z_L u_L \quad \text{with } Z_L = \rho_L c_L.$$

The upperscript '*' stands for the perturbated state.

The velocity and pressure solution of the Riemann problem are thus easily obtained with the help of the interface conditions:

$$(\alpha_1 p_1 + \alpha_2 p_2)_L^* = (\alpha_1 p_1 + \alpha_2 p_2)_R^* = (\alpha_1 p_1 + \alpha_2 p_2)^* = p^*,$$
$$u_L^* = u_R^* = u^*.$$

The velocity and pressure solution of the Riemann problem read:

$$\begin{aligned} u^* &= \frac{Z_L u_L + Z_R u_R + p_L - p_R}{Z_L + Z_R}, \\ p^* &= \frac{Z_L p_R + Z_R p_L + Z_R Z_L (u_L - u_R)}{Z_L + Z_R}. \end{aligned} \tag{III.3}$$

With

$$p = \alpha_1 p_1 + \alpha_2 p_2, \quad Z = \rho c, \quad \rho = \alpha_1 \rho_1 + \alpha_2 \rho_2, \quad c^2 = Y_1 c_1^2 + Y_2 c_2^2.$$

Relations (III.3) are the same for the 6-equation model and for the Euler equations. The differences appear through the definitions of the mixture pressure, mixture sound speed and mixture density.

Once the pressure is determined in the star region the phase's densities are determined with the help of the entropy jumps.

This solver is simple and efficient for subsonic flows or flows in absence of strong shocks. Characteristic relations are also useful for boundary conditions treatment. But we prefer a solver able to deal with arbitrary shocks, genuinely positive (and consequently robust), able to deal with arbitrary convex EOS. The HLLC solver of Toro et al. [51] fulfils these requirements.

3.1.2. HLLC-type solver

Consider a cell boundary separating a left state (L) and a right state (R). The left- and right-facing waves speeds are readily obtained, following Davis [12] estimates:

$$S_R = \max(u_L + c_L, u_R + c_R), \quad S_L = \min(u_L - c_L, u_R - c_R),$$

where the sound speed still obeys to Relation (III.2).

The speed of the intermediate wave (or contact discontinuity) is estimated using the HLL approximation

$$S_M = \frac{(\rho u^2 + p)_L - (\rho u^2 + p)_R - S_L(\rho u)_L + S_R(\rho u)_R}{(\rho u)_L - (\rho u)_R - S_L \rho_L + S_R \rho_R},$$

with the mixture density and mixture pressure defined previously.

From these wave speeds, the following variable states are determined

$$(\alpha_k\rho_k)^*_R = (\alpha_k\rho_k)_R \frac{S_R - u_R}{S_R - S_M},$$
$$(\alpha_k\rho_k)^*_L = (\alpha_k\rho_k)_L \frac{S_L - u_L}{S_L - S_M},$$
$$p^* = p_R + \rho_R u_R (u_R - S_R) - \rho^*_R S_M (S_M - S_R), \quad \text{with } \rho^*_R = \sum_k (\alpha_k\rho_k)^*_R,$$
$$E^*_R = \frac{\rho_R E_R (u_R - S_R) + p_R u_R - p^* S_M}{\rho^*_R (S_M - S_R)},$$
$$E^*_L = \frac{\rho_L E_L (u_L - S_L) + p_L u_L - p^* S_M}{\rho^*_L (S_M - S_L)}, \quad \text{with } E = Y_1 e_1 + Y_2 e_2 + \frac{1}{2}u^2.$$

The volume fraction jump is readily obtained, as in the absence of relaxation effects the volume fraction is constant along fluid trajectories

$$\alpha^*_{kR} = \alpha_{kR}, \quad \alpha^*_{kL} = \alpha_{kL}.$$

As the volume fraction is constant across left- and right-facing waves, the fluid density is determined from the preceding relations:

$$\rho^*_{kR} = \rho_{kR} \frac{u_R - S_R}{S_M - S_R}.$$

Internal energy jumps are determined with the help of the Hugoniot relation (II.8). Let us consider the example of fluids governed by the stiffened gas EOS (II.3). With the help of the EOS, the phasic pressures are constrained along their Hugoniot curves to be functions only of the corresponding phase density:

$$p^*_k(\rho^*_k) = (p_k + p_{\infty k}) \frac{(\gamma_k - 1)\rho_k - (\gamma_k + 1)\rho^*_k}{(\gamma_k - 1)\rho^*_k - (\gamma_k + 1)\rho_k} - p_{\infty k}.$$

The phase's internal energies are then determined from the EOS: $e^*_{kR} = e^*_{kR}(p^*_k, \rho^*_k)$.

Equipped with these approximate Riemann solvers, the next step is to develop a Godunov type scheme.

3.2. Godunov type method

For the sake of simplicity, the method is presented at first-order. The extension to second-order is detailed in Appendix C.

3.2.1. First-order method

In the absence of relaxation terms, the conservative part of System (III.1) is updated with the conventional Godunov scheme:

$$U^{n+1}_i = U^n_i - \frac{\Delta t}{\Delta x}(F^*(U^n_i, U^n_{i+1}) - F^*(U^n_{i-1}, U^n_i)),$$

where $U = ((\alpha\rho)_1, (\alpha\rho)_2, \rho u, \rho E)^{\mathrm{T}}$ and $F = ((\alpha\rho)_1 u, (\alpha\rho)_1 u, \rho u^2 + p, (\rho E + p)u)^{\mathrm{T}}$, $E = Y_1 e_1 + Y_2 e_2 + \frac{1}{2}u^2$ and $p = \alpha_1 p_1 + \alpha_2 p_2$.

The volume fraction equation is also updated using the Godunov method for advection equations:

$$\alpha^{n+1}_{1i} = \alpha^n_{1i} - \frac{\Delta t}{\Delta x}((u\alpha_1)^*_{i+1/2} - (u\alpha_1)^*_{i-1/2} - \alpha^n_{1i}(u^*_{i+1/2} - u^*_{i-1/2})).$$

This scheme guarantees volume fraction positivity during the hyperbolic step. Other options are possible, like for example, VOF type methods [32]. Using a reconstruction algorithm may have nice features when dealing with interfaces *only*, these interfaces having to be present at the initial time. As we also deal with dynamic appearance of interfaces, a capturing method is preferred. This is not the only difference between the Miller and Puckett [32] method and the present one. The mixture pressure and sound speed used in the present formulation are very different from the single phase estimates used by these authors.

Regarding the non-conservative energy equations, there is no hope to determine accurate approximation in the presence of shocks [22]. Therefore, we use the simplest approximation of the corresponding equations by assuming the product $(\alpha p)^n_{ki}$ constant during the time step:

$$(\alpha\rho e)^{n+1}_{ki} = (\alpha\rho e)^n_{ki} - \frac{\Delta t}{\Delta x}((\alpha\rho eu)^*_{ki+1/2} - (\alpha\rho eu)^*_{ki-1/2} + (\alpha p)^n_{ki}(u^*_{i+1/2} - u^*_{i-1/2})).$$

The lack of accuracy in the internal energy computation resulting from the present scheme is not so crucial. The internal energies will be used only to estimate the phase's pressure at the end of the hyperbolic step, before the relaxation one. The relaxation step will give a first correction to the internal energies, in agreement with the second law of thermodynamics.

A second correction will be made with the help of the total mixture energy. The details of these two steps are described in the next two subsections. Before giving these details, let us examine a basic situation of fundamental importance when dealing with interface problems; namely uniform flow conditions.

3.2.2. Uniform flow test

The main difficulty in solving interface problems as diffused numerical zones lies in the building of a flow model and a numerical scheme that preserve interface conditions. The uniform flow test problem was proposed by Abgrall [1] in the context of the Euler equations. Let us consider a one-dimensional flow in mechanical equilibrium. A volume fraction discontinuity propagates at constant velocity u in a constant pressure flow field $p_1 = p_2 = p$. This flow system is initially in mechanical equilibrium and therefore must remain in mechanical equilibrium during its time evolution.

Let us examine the behavior of the present Godunov method for the conservative part of this model in the particular case of uniform pressure and velocity fields. The Godunov method for the mass equations is:

$$(\alpha\rho)_{ki}^{n+1} = (\alpha\rho)_{ki}^{n} - \frac{\Delta t}{\Delta x}((\alpha\rho u)^{*}_{ki+1/2} - (\alpha\rho u)^{*}_{ki-1/2}), \quad k = 1,2.$$

Because the velocity is uniform we have:

$$(\alpha\rho)_{ki}^{n+1} = (\alpha\rho)_{ki}^{n} - \frac{\Delta t}{\Delta x}u((\alpha\rho)^{*}_{ki+1/2} - (\alpha\rho)^{*}_{ki-1/2}).$$

The mixture density thus obeys to the discrete formula:

$$\rho_{i}^{n+1} = \rho_{i}^{n} - \frac{\Delta t}{\Delta x}u(\rho^{*}_{i+1/2} - \rho^{*}_{i-1/2}).$$

The discrete momentum equation under the same uniform flow conditions becomes

$$(\rho u)_{i}^{n+1} = (\rho u)_{i}^{n} - \frac{\Delta t}{\Delta x}u^{2}(\rho^{*}_{i+1/2} - \rho^{*}_{i-1/2}).$$

That is

$$(\rho u)_{i}^{n+1} = u(\rho)_{i}^{n+1}.$$

Thus the flow will necessarily retain its uniform velocity at the next time step: $u_{i}^{n+1} = u$.

The adopted numerical scheme for the internal energies becomes in the present situation

$$(\alpha\rho e)_{ki}^{n+1} = (\alpha\rho e)_{ki}^{n} - \frac{\Delta t}{\Delta x}u((\alpha\rho e)^{*}_{ki+1/2} - (\alpha\rho e)^{*}_{ki-1/2}).$$

Consider, for example, the stiffened gas (SG) EOS (II.3): $\rho_k e_k = \frac{p_k + \gamma_k p_{\infty k}}{\gamma_k - 1}$.

The discrete approximation of the internal energy now becomes

$$\left(\alpha\frac{p+\gamma p_{\infty}}{\gamma-1}\right)_{ki}^{n+1} = \left(\alpha\frac{p+\gamma p_{\infty}}{\gamma-1}\right)_{ki}^{n} - \frac{\Delta t}{\Delta x}u\left(\left(\alpha\frac{p+\gamma p_{\infty}}{\gamma-1}\right)^{*}_{ki+1/2} - \left(\alpha\frac{p+\gamma p_{\infty}}{\gamma-1}\right)^{*}_{ki-1/2}\right).$$

As the EOS parameters are constant in each fluid, this expression simplifies to:

$$(\alpha(p+\gamma p_{\infty}))_{ki}^{n+1} = (\alpha(p+\gamma p_{\infty}))_{ki}^{n} - \frac{\Delta t}{\Delta x}u((\alpha(p+\gamma p_{\infty}))^{*}_{ki+1/2} - (\alpha(p+\gamma p_{\infty}))^{*}_{ki-1/2}),$$

which can be rewritten as

$$(\alpha p)_{ki}^{n+1} + (\gamma p_{\infty})_{k}(\alpha)_{i}^{n+1} = p\left\{(\alpha)_{ki}^{n} - \frac{\Delta t}{\Delta x}u((\alpha)^{*}_{ki+1/2} - (\alpha)^{*}_{ki-1/2})\right\} + (\gamma p_{\infty})_{k}\left\{(\alpha)_{ki}^{n} - \frac{\Delta t}{\Delta x}u((\alpha)^{*}_{ki+1/2} - (\alpha)^{*}_{ki-1/2})\right\}.$$

The adopted numerical scheme for the volume fraction evolution, in uniform velocity flow conditions becomes:

$$\alpha_{ki}^{n+1} = \alpha_{ki}^{n} - \frac{\Delta t}{\Delta x}u((\alpha_{k})^{*}_{i+1/2} - (\alpha_{k})^{*}_{i-1/2}).$$

Using this, the internal energy equation reduces to:

$$p_{ki}^{n+1} = p.$$

The adopted numerical approximation thus preserves interface conditions in mechanical equilibrium flows.

When the EOS are more sophisticated than the SG one, i.e. Mie Gruneisen EOS for example that can be written under the form,

$$\rho_k e_k = \frac{p_k + \gamma_k p_{\infty k}(\rho_k)}{\gamma_k - 1}.$$

The same properties of interface preserving are observed experimentally. The reason is that Godunov type methods used for mass and volume fraction equations result in prolonged density field through the interface. Locally, these more sophisticated EOS thus reduce to the SG one.

3.3. Relaxation step

This step is of major importance to fulfill interface conditions in *non-uniform* velocity and pressure flows. It also forces the solution of the 6-equation model to converge to that of the 5-equation model.

In the relaxation step we must solve

$$\begin{aligned}
&\frac{\partial \alpha_1}{\partial t} = \mu(p_1 - p_2),\\
&\frac{\partial \alpha_1\rho_1 e_1}{\partial t} = -p_I\mu(p_1 - p_2),\\
&\frac{\partial \alpha_2\rho_2 e_2}{\partial t} = p_I\mu(p_1 - p_2),\\
&\frac{\partial \alpha_1\rho_1}{\partial t} = 0,\\
&\frac{\partial \alpha_2\rho_2}{\partial t} = 0,\\
&\frac{\partial \rho u}{\partial t} = 0,\\
&\frac{\partial \rho E}{\partial t} = 0
\end{aligned}$$

with $p_I = \frac{Z_2 p_1 + Z_1 p_2}{Z_1 + Z_2}$ and in the limit $\mu \to +\infty$.

After some manipulations the internal energy equations become

$$\begin{aligned}
&\frac{\partial e_1}{\partial t} + p_I \frac{\partial v_1}{\partial t} = 0,\\
&\frac{\partial e_2}{\partial t} + p_I \frac{\partial v_2}{\partial t} = 0.
\end{aligned}$$

This system can be written in integral formulation

$$e_k - e_k^0 + \hat{p}_{Ik}(v_k - v_k^0) = 0,$$

where $\hat{p}_{Ik} = \frac{1}{v_k - v_k^0}\int_0^{\Delta t} p_I \frac{\partial v_k}{\partial t} dt$.

Determination of pressure averages $\hat{p}_{Ik}$ has to be done in agreement with thermodynamic considerations. By summing the internal energy equations we have:

$$Y_1 e_1 - Y_1 e_1^0 + Y_2 e_2 - Y_2 e_2^0 + \hat{p}_{I1}(Y_1 v_1 - Y_1 v_1^0) + \hat{p}_{I2}(Y_2 v_2 - Y_2 v_2^0) = 0.$$

The mixture mass equation can be written as

$$(Y_1 v_1 - Y_1 v_1^0) + (Y_2 v_2 - Y_2 v_2^0) = 0.$$

Using these relations the mixture energy equation becomes

$$e - e^0 + (\hat{p}_{I1} - \hat{p}_{I2})(Y_1 v_1 - Y_1 v_1^0) = 0.$$

In order that the mixture energy conservation be fulfilled it is necessary that: $\hat{p}_{I1} = \hat{p}_{I2} = \hat{p}_I$. Possible estimates are $\hat{p}_I = p_I^0$ or $\hat{p}_I = p$, the initial and relaxed pressures respectively. These estimates are compatible with the entropy inequality [43]. With regard to the choice of one or the other estimate, upon computation of the relaxed state the resulting difference in practical computations is negligible. This negligible influence will be illustrated in the results section. The system to solve is thus composed of equations

$$e_k(p, v_k) - e_k^0(p_k^0, v_k^0) + \hat{p}_I(v_k - v_k^0) = 0, \quad k = 1, 2,$$

which involves 3 unknowns, $v_k (k = 1,2)$ and p. Its closure is achieved using the saturation constraint

$$\sum_k \alpha_k = 1,$$

or

$$\sum_k (\alpha\rho)_k v_k = 1.$$

Here the $(\alpha\rho)_k$ are constant during the relaxation process. This system can be replaced by a single equation with a single unknown (p). With the help of the EOS (II.3) the energy equations become

$$v_k(p) = v_k^0 \frac{p^0 + \gamma_k p_{\infty k} + (\gamma_k - 1)\hat{p}_I}{p + \gamma_k p_{\infty k} + (\gamma_k - 1)\hat{p}_I},$$

and thus the only equation to solve (for p) is

$$\sum_k (\alpha\rho)_k v_k(p) = 1. \tag{III.4}$$

Once the relaxed pressure is found, the phase's specific volumes and volume fractions are determined.

In the Miller and Puckett [32] method, the relaxed pressure is used to advance the solution to the next time step. However, there is no guarantee that the mixture EOS or the mixture energy be in agreement with this relaxed pressure. In order to respect total energy and correct shock dynamics on both sides of the interface, the following correction is employed.

3.4. Reinitialization step

As the volume fractions have been estimated previously by the relaxation method, the mixture pressure can be determined from the mixture EOS based on the mixture energy which is known from the solution of the total energy equation. Because the mixture total energy obeys a conservation law, its evolution is accurate in the entire flow field and in particular at shocks.

Again considering fluids governed by the stiffened gas EOS, the mixture EOS in this context relates mixture energy, density and volume fractions (II.4):

$$p(\rho, e, \alpha_1, \alpha_2) = \frac{\rho e - \left(\frac{\alpha_1 \gamma_1 p_{\infty 1}}{\gamma_1 - 1} + \frac{\alpha_2 \gamma_2 p_{\infty 2}}{\gamma_2 - 1}\right)}{\frac{\alpha_1}{\gamma_1 - 1} + \frac{\alpha_2}{\gamma_2 - 1}}.$$

This EOS is valid in pure fluids and in the diffuse interface zone. As it is valid in pure fluids, and based on the total energy equation, it guarantees correct and conservative wave dynamics on both sides of the interface. Inside the numerical diffusion zone of the interface, numerical experiments show that the method is accurate too, as the volume fractions used in the mixture EOS (II.4) have a quite accurate prediction from the relaxation method.

Once the mixture pressure is determined from (II.4) the internal energies of the phases are reinitialized with the help of their respective EOS before going to the next time step

$$e_k = e_k(p, \alpha_k \rho_k, \alpha_k). \tag{III.5}$$

3.5. Summary

The numerical method can be summarized as follows:

- At each cell boundary solve the Riemann problem of System (III.1) with favorite solver. The HLLC solver of Section 3.1 is recommended.
- Evolve all flow variables with the Godunov type method of Section 3.2.
- Determine the relaxed pressure and especially the volume fraction by solving Eq. (III.4). The Newton method is appropriate for this task.
- Compute the mixture pressure with Eq. (II.4).
- Reset the internal energies with the computed pressure with the help of their respective EOS (III.5).
- Go to the first item for the next time step.

4. Tests and validations

4.1. Advection of an interface in a uniform pressure and velocity flow

A discontinuity of volume fraction (thus a mixture density discontinuity) is moving in a uniform pressure and velocity flow at 100 m/s. Initially the discontinuity is located at $x = 0.5$ m in a 1 m length tube. This discontinuity separates two nearly pure fluids, liquid water on the left defined by $\rho_{\text{water}} = 1000\ \text{kg m}^{-3}$, and the stiffened gas EOS parameters $\gamma_{\text{water}} = 4.4$, $p_{\infty,\text{water}} = 6 \times 10^8$ Pa and air on the right defined by $\rho_{\text{air}} = 10\ \text{kg m}^{-3}$ with the ideal gas EOS parameters $\gamma_{\text{air}} = 1.4$ and $p_{\infty,\text{air}} = 0$ Pa. In the left chamber, the water volume fraction is set to $\alpha_{\text{water}} = 1 - \varepsilon$ and in the right chamber its value is $\alpha_{\text{water}} = \varepsilon$, with $\varepsilon = 10^{-8}$. The uniform pressure is set equal to $p = 10^5$ Pa.

The numerical solution is plotted in Fig. 5 at time $t = 2.79$ ms and is compared to the exact one. A mesh with 200 uniform cells is used with a second-order extension of the method (see Appendix C for details).

The agreement between the numerical and analytical solutions is excellent and the numerical solution is oscillation free, except for the Mach number, computed with the equilibrium sound speed c_{eq}. For this test case, the flow being in mechanical equilibrium, relaxation terms present in the volume fraction and energy equations have no importance, as well as the pres-

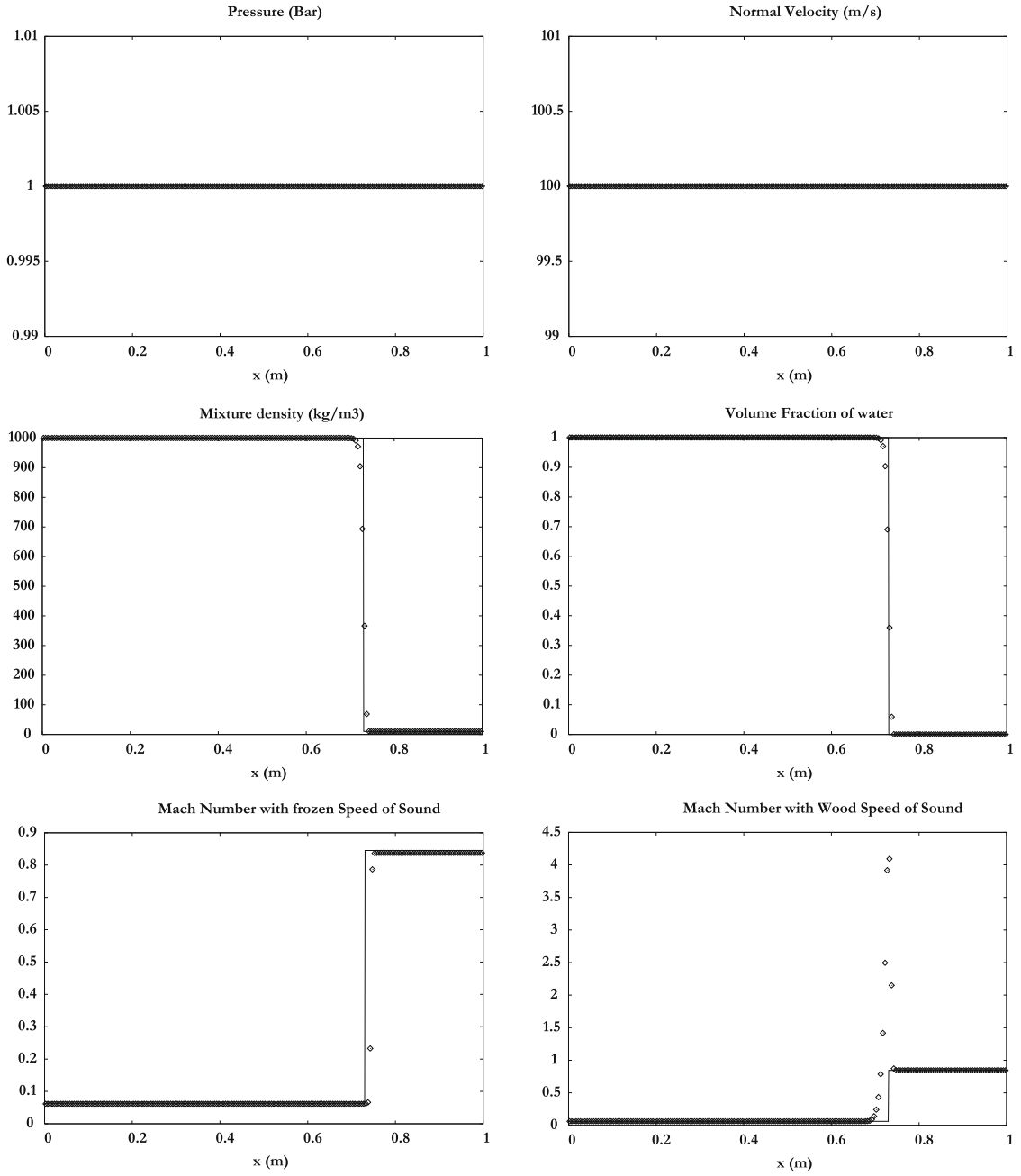

Fig. 5. Advection of a volume fraction discontinuity in a uniform pressure and velocity flow. Comparison of the relaxation method with Superbee limiter (symbols) and the exact solution (solid). A 200 cells mesh is used. Excellent agreement is observed.

sure relaxation step. The respect of interface conditions is just a consequence of the clean numerical approximation with the Godunov method of conservative and non-conservative equations of Section 3.2.

4.2. Shock tube with Mie-Grüneisen type EOS

In order to show the method's capabilities, in particular when dealing with more general equations of state, a test involving the [9] EOS (CC EOS) is considered. This EOS is of Mie-Grüneisen type. The same shock tube problem presented in Saurel et al. [43] is considered. In this example, a single fluid is considered governed by CC EOS, with a density discontinuity in a shock tube. As there is a single fluid, the Godunov method is expected to be valid. However, it was shown in the same reference that due to the nonlinearity of $p_\infty(\rho)$ in the EOS, the Godunov method produced pressure and velocity oscillations. A cure to these difficulties was proposed in that same reference. Here, with the help of the multiphase flow model, these

difficulties can be solved by considering the single fluid as a two-phase media with the initial discontinuity in the shock tube separating the two states.

Initially, the high pressure chamber is set to 20 GPa, while the pressure is set equal to 0.2 MPa in the low pressure chamber. Both chambers are filled with liquid nitromethane, governed by the CC EOS in which densities are respectively set to 1134 kg m^{-3} and 1200 kg m^{-3}. In the high pressure chamber, volume fraction of the first phase is set to $\alpha_1 = 1 - \varepsilon$ and in the right chamber its value is $\alpha_1 = \varepsilon$ ($\varepsilon = 10^{-8}$). Thus, the model is used in the single phase limit, i.e. the same EOS is used for both fluids but with different initial densities:

$$p(\rho, e) = \rho\Gamma(e - e_k(\rho)) + p_k(\rho),$$

with

$$e_k(\rho) = \frac{A_1}{\rho_{ref}(E_1 - 1)}\left(\frac{\rho}{\rho_{ref}}\right)^{E_1 - 1} - \frac{A_2}{\rho_{ref}(E_2 - 1)}\left(\frac{\rho}{\rho_{ref}}\right)^{E_2 - 1},$$

$$p_k(\rho) = A_1\left(\frac{\rho}{\rho_{ref}}\right)^{E_1} - A_2\left(\frac{\rho}{\rho_{ref}}\right)^{E_2}.$$

The data used in the present simulation are: $\Gamma = 1.19$, $\rho_{\text{ref}} = 1134$ kg m^{-3}, $A_1 = 0.819181 \times 10^9$ Pa, $A_2 = 1.50835 \times 10^9$ Pa, $E_1 = 4.52969$ and $E_2 = 1.42144$.

The solution is presented at time $t = 67$ μs in Fig. 6. The present relaxation method is compared to the exact solution of the Euler equations. Results are similar to those of Saurel et al. [43] but the present algorithm is easier to implement. A magnified view of pressure and velocity around the contact discontinuity is given in Fig. 7. It presents a solution free of oscillations.

4.3. Water–air shock tubes

4.3.1. Water–air shock tube with moderate pressure ratio and high density ratio

A 1 m long shock tube containing two chambers separated by an interface at the location $x = 0.75$ m is considered. Each chamber contains a nearly pure fluid. The initial density of water is $\rho_{\text{water}} = 1000$ kg m^{-3} and the stiffened gas EOS parameters are $\gamma_{\text{water}} = 4.4$ and $p_{\infty,\text{water}} = 6 \times 10^8$ Pa. The initial density of air is $\rho_{\text{air}} = 1$ kg m^{-3} and EOS parameters are $\gamma_{\text{air}} = 1.4$ and

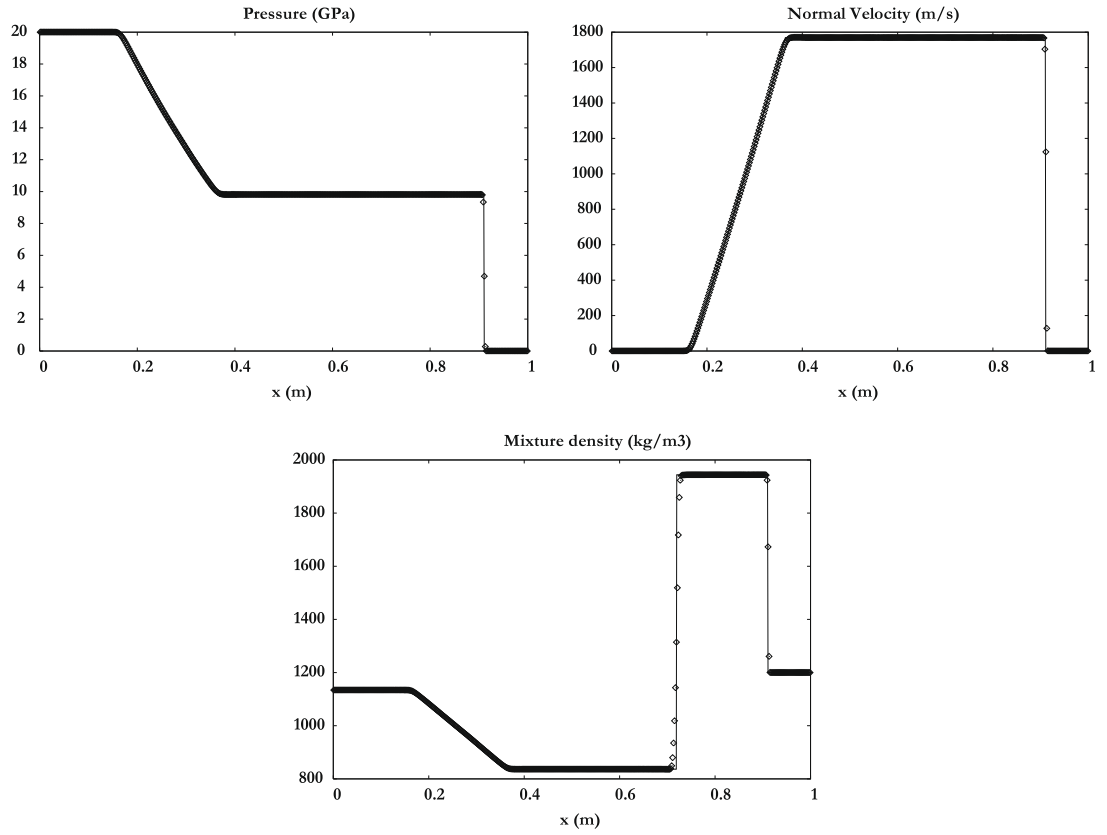

Fig. 6. Shock tube with Mie-Grüneisen type EOS. The present relaxation method based on the 6-equation model (symbols) is compared to the exact solution of the Euler equations (solid). A 500 cells mesh is used. Results are in perfect agreement.

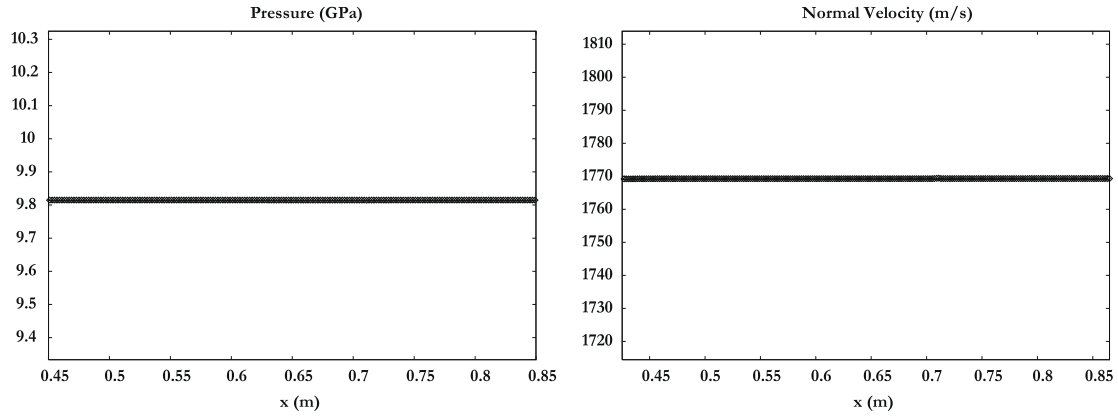

Fig. 7. Shock tube with Mie-Grüneisen type EOS. Magnified view of pressure and density around the contact discontinuity. Results are in perfect agreement with the exact solution and the solution is oscillation free.

$p_{\infty,\,\mathrm{air}} = 0$ Pa. The left chamber contains a very small volume fraction of air $\alpha_{\mathrm{air}} = 10^{-6}$ and the initial pressure is set equal to 1 GPa. The right chamber contains the same fluids but the volume fractions are reversed. The initial pressure is set equal to 0.1 MPa. In both chambers the initial velocity is equal to 0.

The numerical solution of the 6-equation model is compared to the exact solution of the Euler equations. A mesh employing 1000 uniform cells is used in Fig. 8 and a mesh employing 100 cells is used in Fig. 9. Comparison with the exact solution is shown in both figures at time $t = 240$ μs. Again this test poses no computational difficulty.

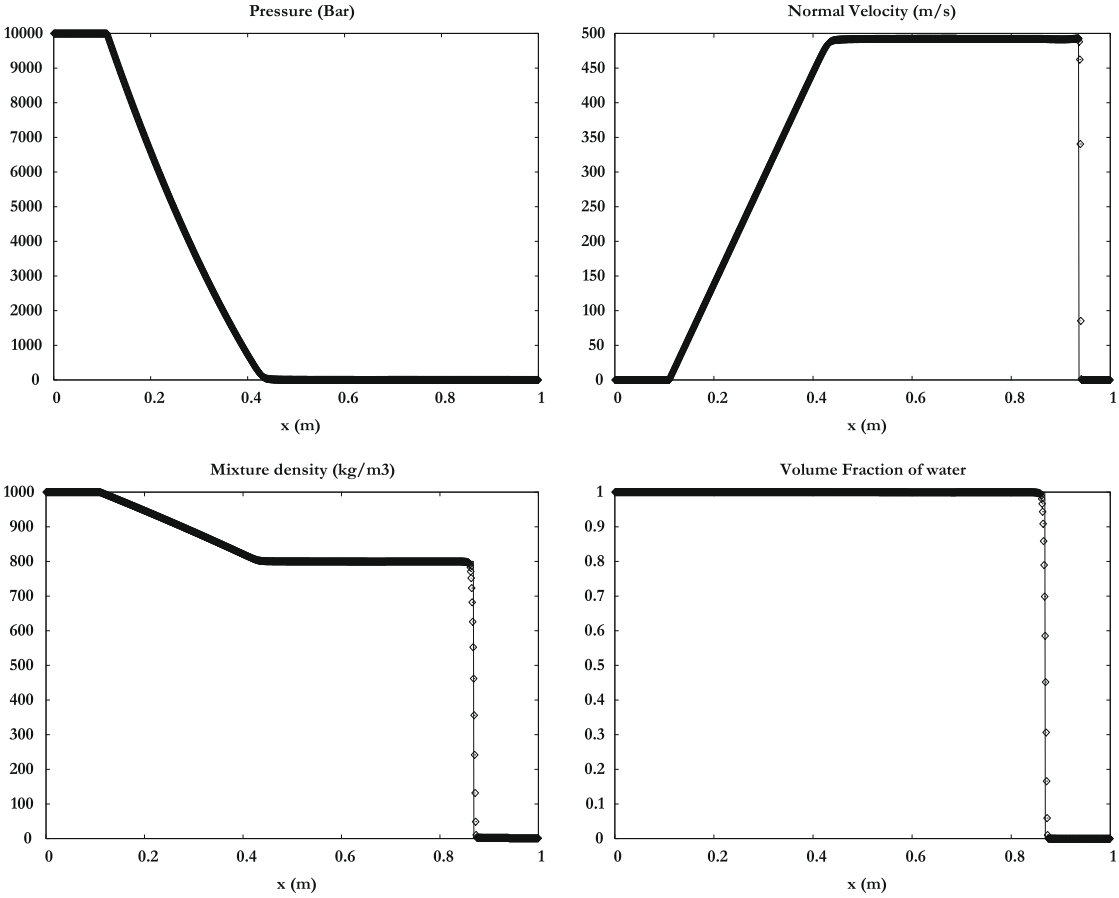

Fig. 8. Liquid/gas shock tube. The present relaxation method is used to solve the 6-equation model. Numerical results are shown with symbols and compared to the exact solution (solid). A 1000 cells mesh is used. The density ratio is 1000 and the pressure ratio is 10,000 at the initial discontinuity. A second-order extension of the method with van Leer limiter is used. Results are in excellent agreement.

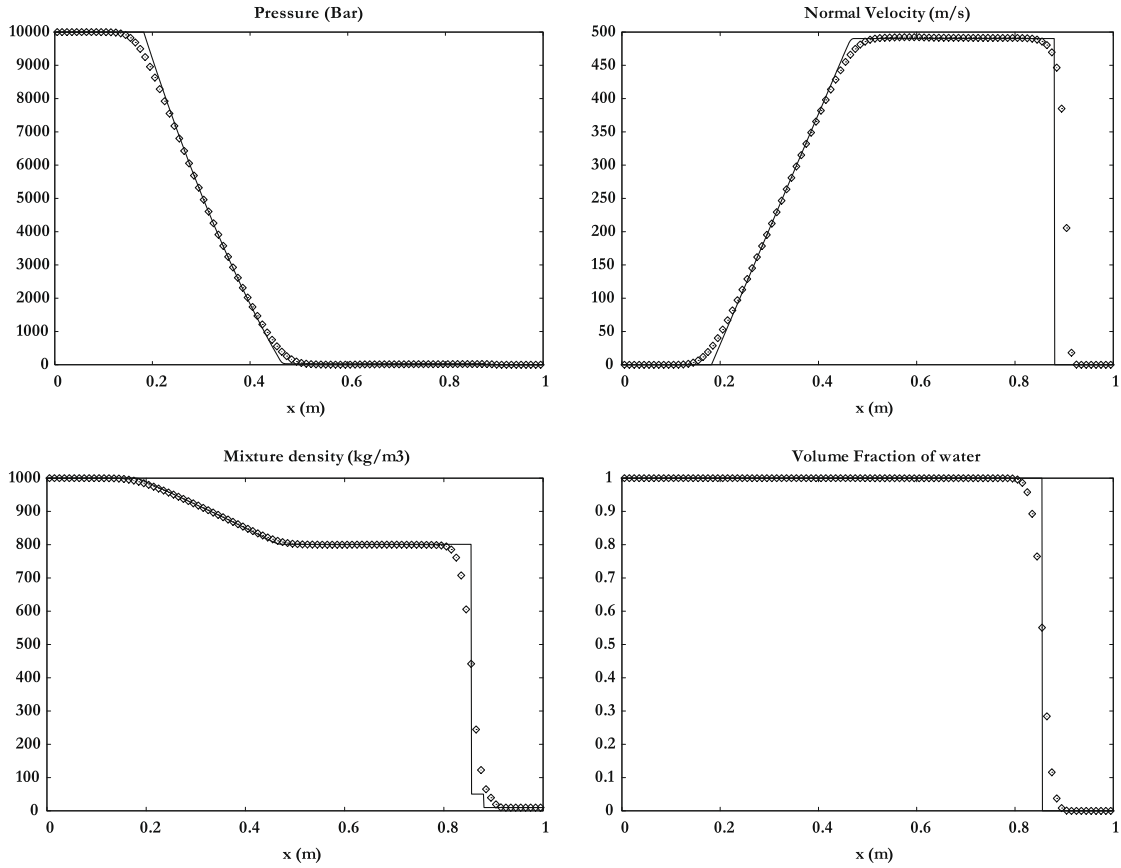

Fig. 9. Same liquid/gas shock tube as those of Fig. 8 with 100 cells. Numerical results are shown with symbols and compared to the exact solution (solid). A second-order extension of the method with van Leer limiter is used. Results are in good agreement.

In this test case and in all subsequent tests, strong pressure waves propagate. Relaxation terms present in the volume fraction and energy equations become important, as well as the pressure relaxation step. Robustness and convergence of the algorithm in the unsteady building of the solution are improved by pressure relaxation.

4.3.2. Water–air shock tube in extreme conditions

The same shock tube problem is solved, but initially, the left chamber pressure is set to 1 TPa (10 Mbars) and the density of air is set to 10 kg m^{-3}. The exact solutions of the single phase Euler equations and the multiphase flow model with 6 equations are compared in Fig. 10 at time $t = 8.3$ μs. This test illustrates the robustness and convergence of the algorithm.

4.4. Influence of $\hat{p}_I$ in the relaxation method

During the relaxation step, we have highlighted different possible estimates for the pressure average $\hat{p}_I$. In order to demonstrate the weak influence of the estimate, the liquid/gas shock tube test presented in Fig. 8 is examined with different estimates of $\hat{p}_I$. In Fig. 11, results are presented and compared with two possible estimates: $\hat{p}_I = p_I^0$ or $\hat{p}_I = p$. No differences are visible.

4.5. Cavitation test

A 1 m length tube is filled with liquid water at atmospheric pressure and with density $\rho = 1000$ kg m^{-3}. A small volume fraction of air ($\alpha_{air} = 10^{-2}$) is initially present everywhere. An initial velocity discontinuity is located at $x = 0.5$ m. On the left, the velocity is set to $u = -100$ m/s and on the right, $u = 100$ m/s. Solution is shown in Fig. 12 at time $t = 1.85$ ms, using 1000 uniform mesh cells.

Strong rarefaction waves propagate in the tube and the liquid pressure decreases. As gas is present, the pressure cannot become negative. To maintain positive pressure, the gas volume fraction increases and creates a cavitation pocket. This results in the dynamic appearance of two interfaces that were not present initially. Excellent agreement with the exact solution of the 5-equation model [37] is obtained. Interface creation is readily handled by the present algorithm.

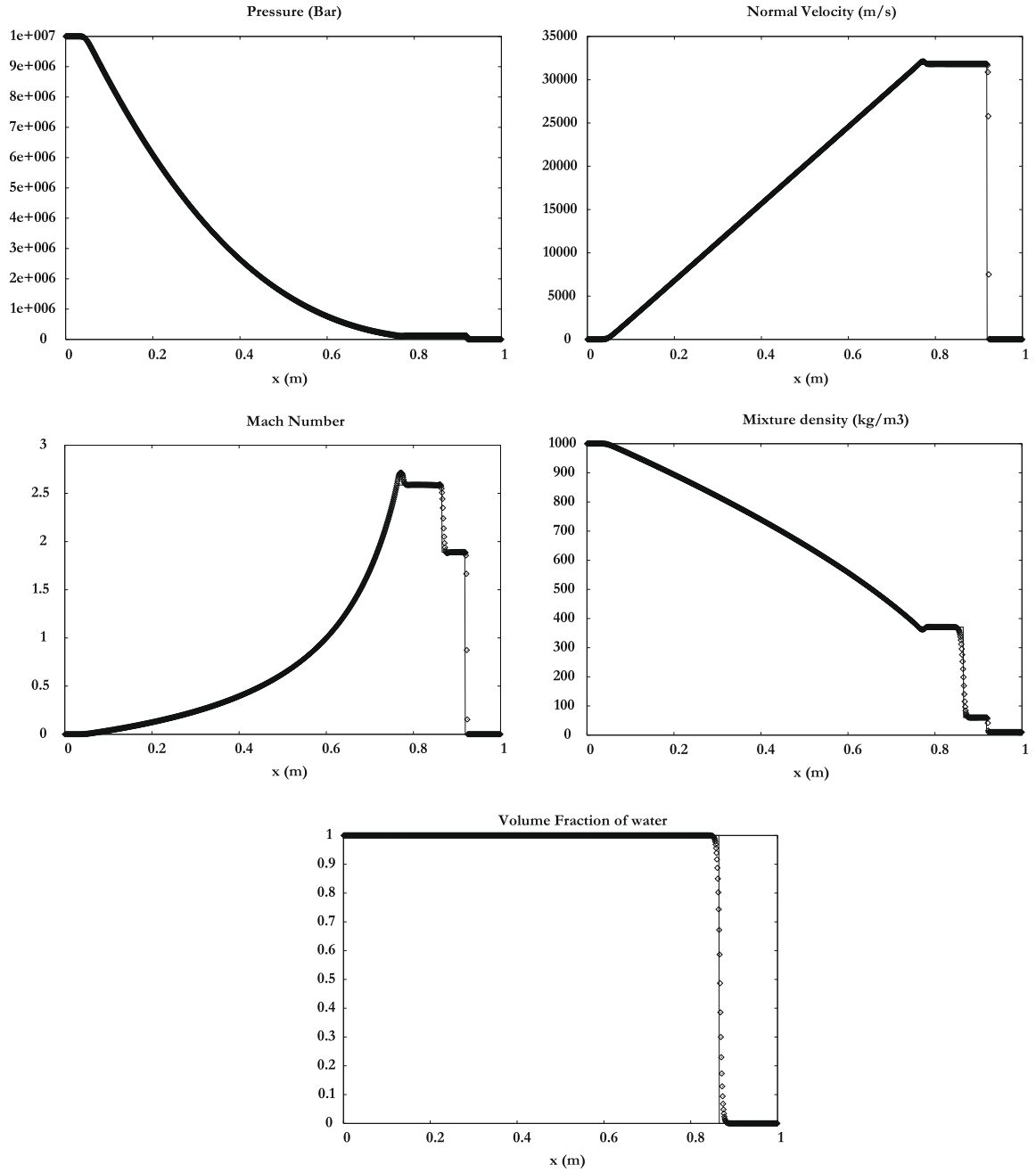

Fig. 10. Liquid/gas shock tube. The present relaxation method is used to solve the 6-equation model. Numerical results are shown with symbols and are compared to the exact solution (solid). A 1000 cells mesh is used. The initial density ratio is 100 and the initial pressure ratio is 10^7. This test illustrates robustness and convergence of the algorithm.

4.6. Multidimensional validation: shock–bubble interaction

Multidimensional finite volume extension of the method is presented in Appendix D. The method is validated against shock tube experiments of shock–bubble interaction. The experiment is one of those proposed in Layes and Le Métayer [27] where full description of the experimental setup is provided. The configuration under study consists in a shock wave propagating at Mach number 1.5 into air at atmospheric conditions and interacting with a helium bubble. The initial density of air is $\rho_{air} = 1.29\ kg\ m^{-3}$ and the initial density of helium is $\rho_{helium} = 0.167\ kg\ m^{-3}$. In the simulation both fluids are considered as ideal gases with polytropic coefficients $\gamma_{air} = 1.4$ and $\gamma_{helium} = 1.67$.

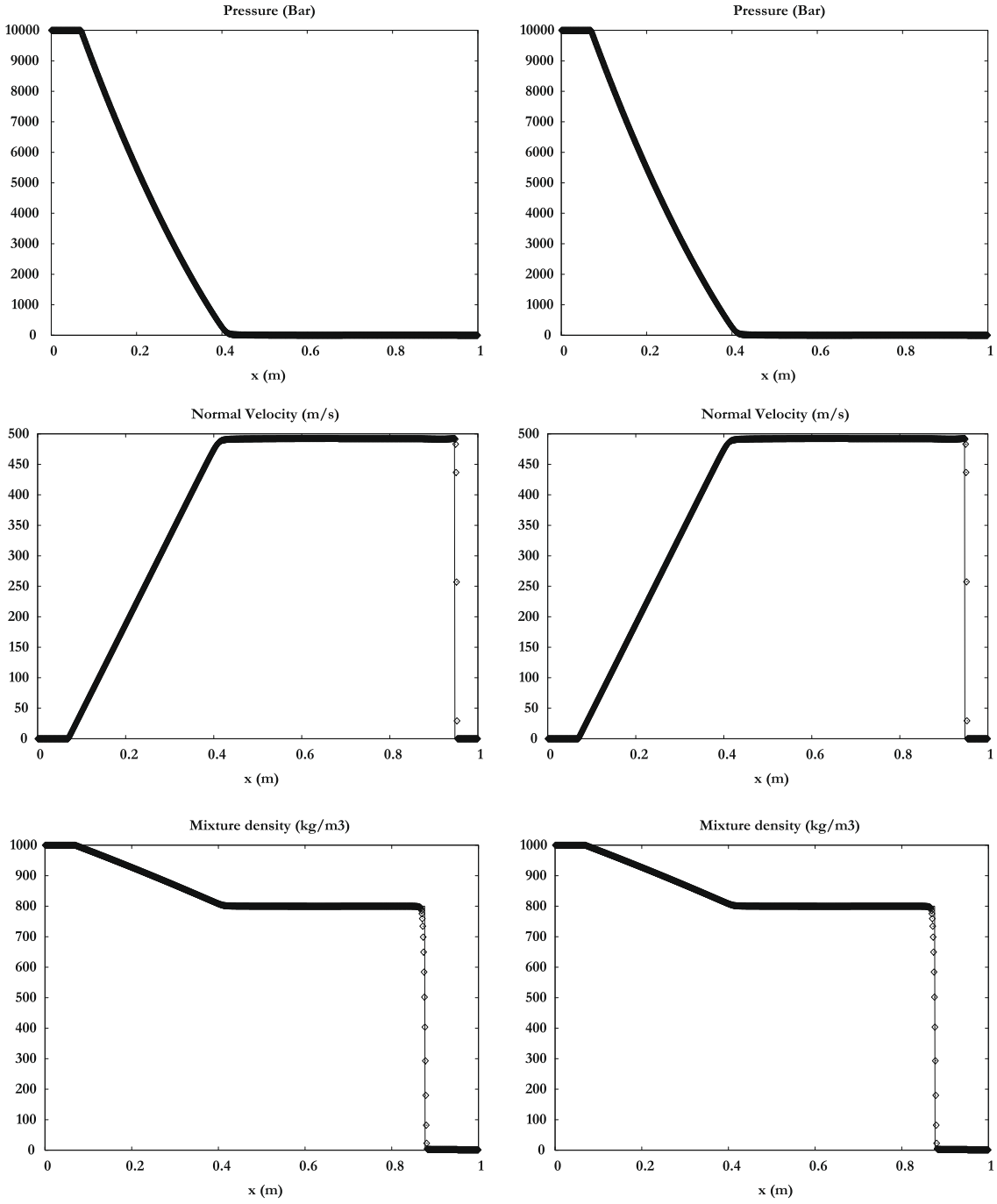

Fig. 11. Comparison of two different pressure averages estimates. The test case of Fig. 8 is computed with $\hat{p}_I = p_I^0$ on the left the and $\hat{p}_I = p$ on the right. From top to bottom, pressure, velocity and mixture density remains unchanged.

The initial configuration is represented in Fig. 13. Computed results are compared with experimental ones in Fig. 14.

4.7. Cavitating Richtmyer–Meshkov instability (RMI)

To illustrate the method capabilities a 2D test involving a RMI with a liquid–gas interface is considered. As the liquid is not pure, new interfaces appear during the development of the instability, due to cavitation effects. The shape of the resulting interface and the entire flow field show a non-conventional behavior, that was never computed before, as the model and method must deal with liquid gas interfaces and dynamic appearance of gas pockets in severe conditions.

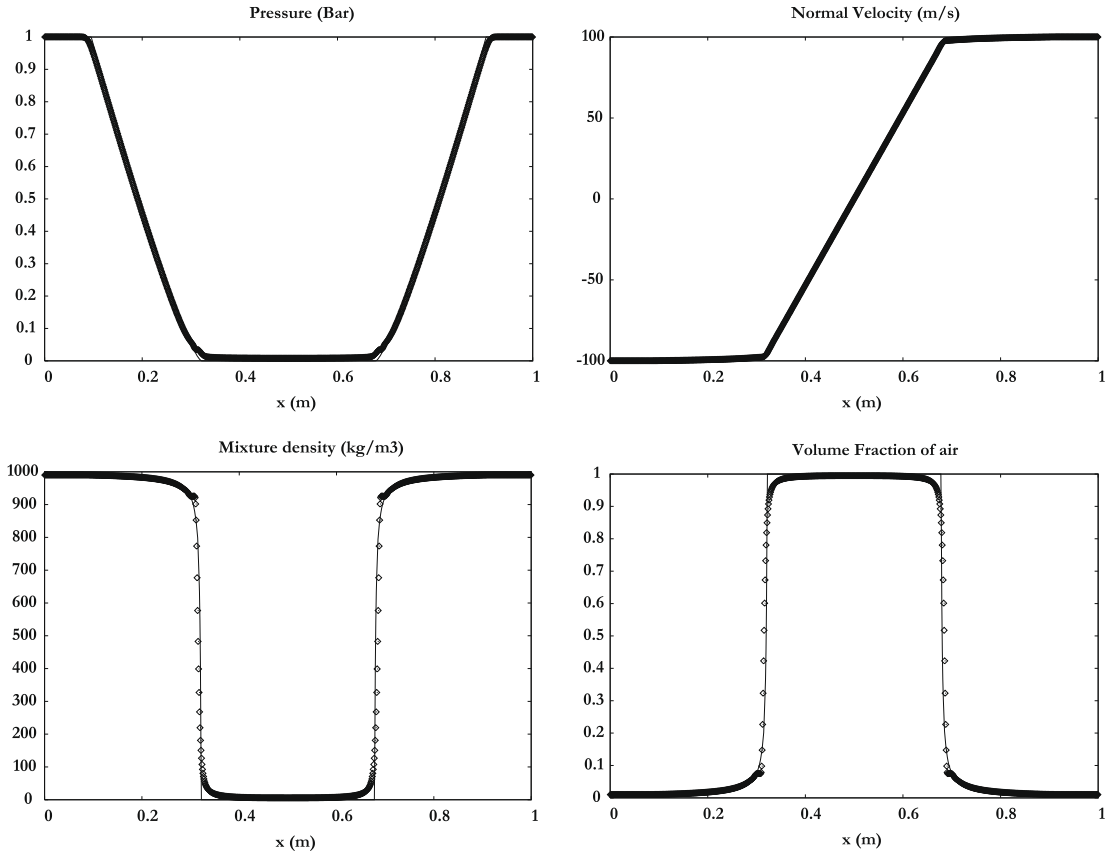

Fig. 12. Expansion tube with cavitation pocket appearance. The present relaxation method is used to solve the 6-equation model. Numerical results are shown with symbols and are compared to the exact solution (solid) of the 5-equation model [37]. A 1000 cells mesh is used.

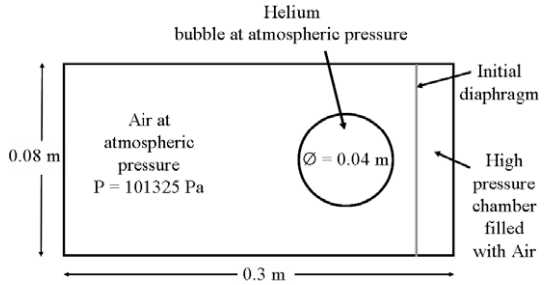

Fig. 13. Initial configuration of the shock–bubble interaction test.

The left part of the computational domain is filled with nearly pure water and the right part with nearly pure gas. They are initially separated by a curved interface. It is a portion of circle with 0.6 m radius centered at $x = 1.2$ m, $y = 0.5$ m. The physical domain is 3 m long and 1 m high. The mesh contains 900 cells along x-direction and 400 cells along y-direction. Both water and gas have an initial velocity of -200 m/s. Top, bottom and left boundaries are treated as solid walls. The initial density of water is $\rho_{water} = 1000$ kg m^{-3} and the stiffened gas EOS parameters are $\gamma_{water} = 4.4$ and $p_{\infty,water} = 6 \times 10^8$ Pa. The initial density of gas is $\rho_{gas} = 100$ kg m^{-3} and EOS parameters are $\gamma_{gas} = 1.8$ and $p_{\infty,gas} = 0$ Pa. The left chamber contains a very small volume fraction of gas $\alpha_{gas} = 10^{-6}$ and the right chamber contains a very small volume fraction of water $\alpha_{water} = 10^{-6}$. The initial configuration is represented in Fig. 15. Results are shown in Fig. 16.

When the flow impacts the left wall, a right-facing shock propagates in the domain through the water/gas discontinuity. A conventional RMI appears first. Then expansion waves are produced as the jet elongates. It results in expanded zones near the solid boundary where gas in-homogeneities grow, producing dynamic appearance of gas pockets. As the pressure is very low in these zones, the jet dynamics is modified compared to conventional RMI with pure fluids. The various gas pockets

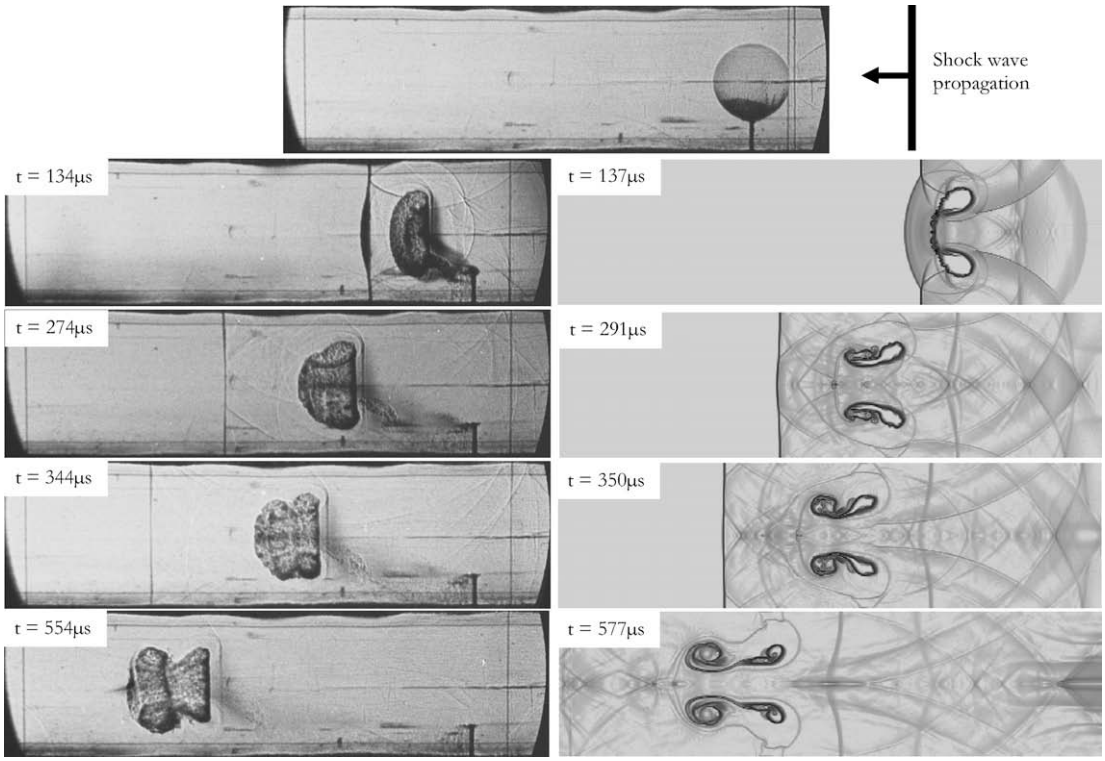

Fig. 14. Shock–bubble interaction test. Experimental results (left) and computed results (right) are compared at different times. Because of the difference in gas properties, the transmitted shock wave is faster than the incident one in air. Pressure and density gradients create vorticity.

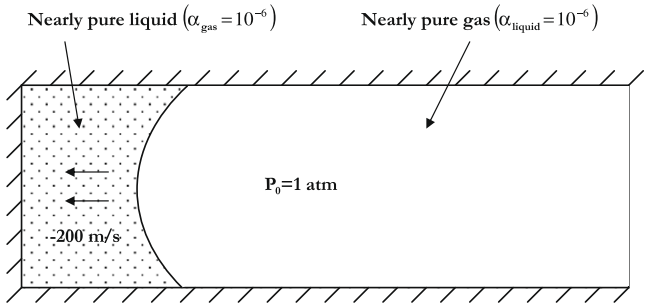

Fig. 15. Initial configuration of the water–gas Richtmyer–Meshkov instability. Both liquid and gas have initial velocity of −200 m/s.

near the solid boundary and in the jet core are clearly visible in Fig. 17 where the gas volume fraction is shown. Relaxation terms present in the volume fraction and energy equations are responsible for the dynamic appearance of these gas pockets.

The link between the 6-equation model and conventional barotropic cavitating flow models that are the most popular in cavitation modeling is detailed in Appendix A. These models are composed of one or two mass conservation equations and one momentum equation. They consist in hyperbolic systems of conservation laws. These models involve an important difficulty related to the non-monotonic behavior of the sound speed versus volume fraction [26,11,48]. It is thus interesting to examine how the various ingredients developed in the context of the 6-equation model can be used for these barotropic models in order to solve this difficulty.

5. Method extension for shocks in multiphase mixtures – artificial heat exchanges

The present refinement of the algorithm is needed only when shock propagation in real multiphase mixtures is under study. For other situations with interfaces separating pure fluids or cavitating flows, there is no need to account for the artificial heat exchanges detailed hereafter. The artificial heat exchange is used to correct the partition of the energies among the various phases in the mixture and to propagate shocks in these mixtures at the correct speed with the correct shocked state.

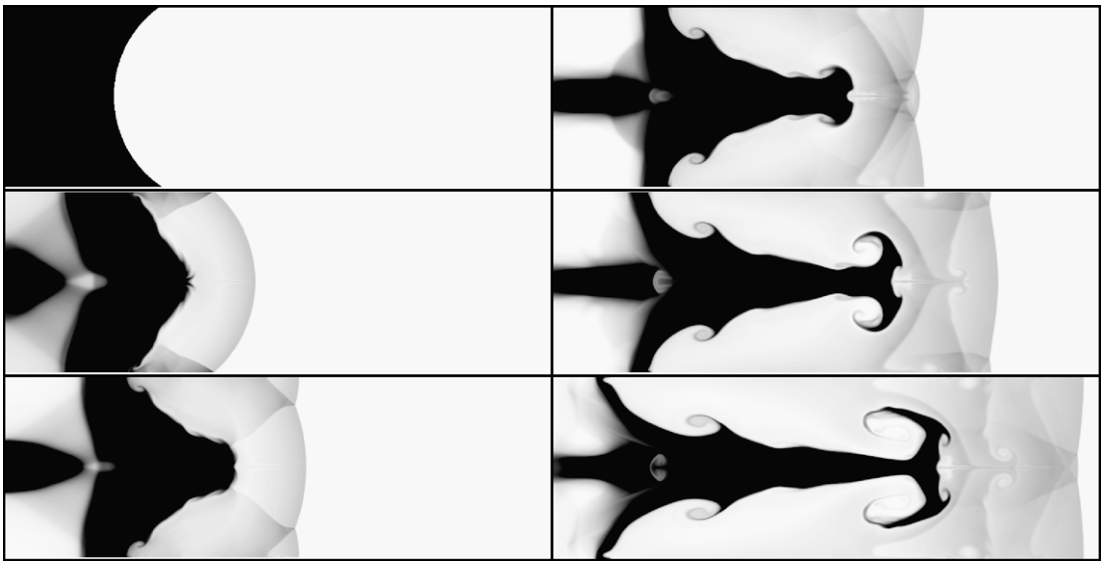

Fig. 16. Water–gas Richtmyer–Meshkov instability. Mixture density contours are shown at time $t_0 = 0$ ms, $t_1 = 2$ ms, $t_2 = 3.1$ ms, $t_3 = 4.8$ ms, $t_4 = 6.4$ ms, $t_5 = 8.6$ ms. The mesh contains 900×400 cells. New interfaces appear dynamically near the solid boundary as a result of expansion waves focusing. They result in cavitation pockets that considerably modify the jet and spike shape.

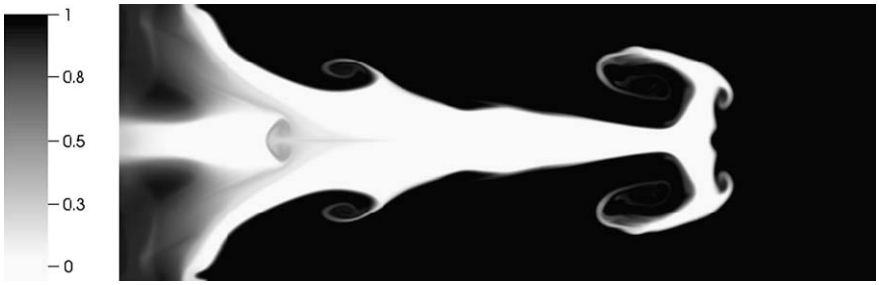

Fig. 17. Water–gas Richtmyer–Meshkov instability. Volume fraction contours of gas are shown at time $t_5 = 8.6$ ms. The gas volume fraction increase into the liquid jet and near the solid wall boundary. The spike shape is also modified.

Some preliminary observations of numerical schemes in the context of single phase flows are first necessary to introduce the numerical issues associated with multiphase shocks.

Consider a shock wave propagating in a pure material, governed by the Euler equations. Shock capturing schemes produce a smearing of discontinuities and it is interesting to compare the thermodynamic path followed by the fluid in the shock layer to the theoretical Hugoniot curve. Such comparison is shown in Fig. 18.

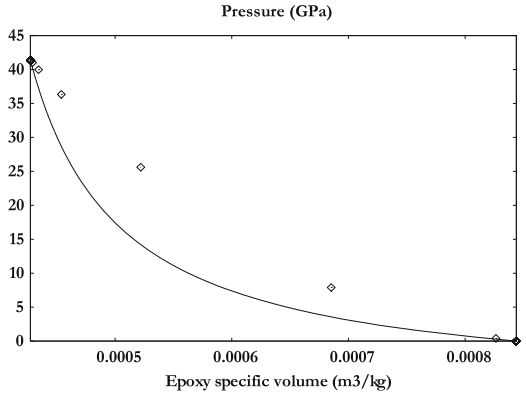

Fig. 18. Comparison of the numerical Hugoniot curve (symbols) and the theoretical one (lines) in the numerical diffusion zone for single phase flows. The two thermodynamic paths are different but the end states are the same.

It appears clearly that the thermodynamic paths are very different. This is due to the succession of numerical weak shocks that propagate into the cell that do not impose the same thermodynamic transformation as a single strong shock [10]. The successive cell averages produce also transformations in disagreement with the single shock Hugoniot.

However, this numerical phenomenon has no consequence on the computation of the shocked state for single phase flows. As shown in Fig. 18, the end of the shock layer merges with the theoretical Hugoniot state. This is a consequence of conservation properties of the Euler equations.

When dealing with multiphase mixtures, the same deviation from the theoretical Hugoniot appears and has more serious consequences. The reason is that for each weak shock that enter the cell, the equation of state changes. Indeed, for multiphase mixtures, there is an extra degree of freedom characterized by the volume fraction. At a given point of the numerical

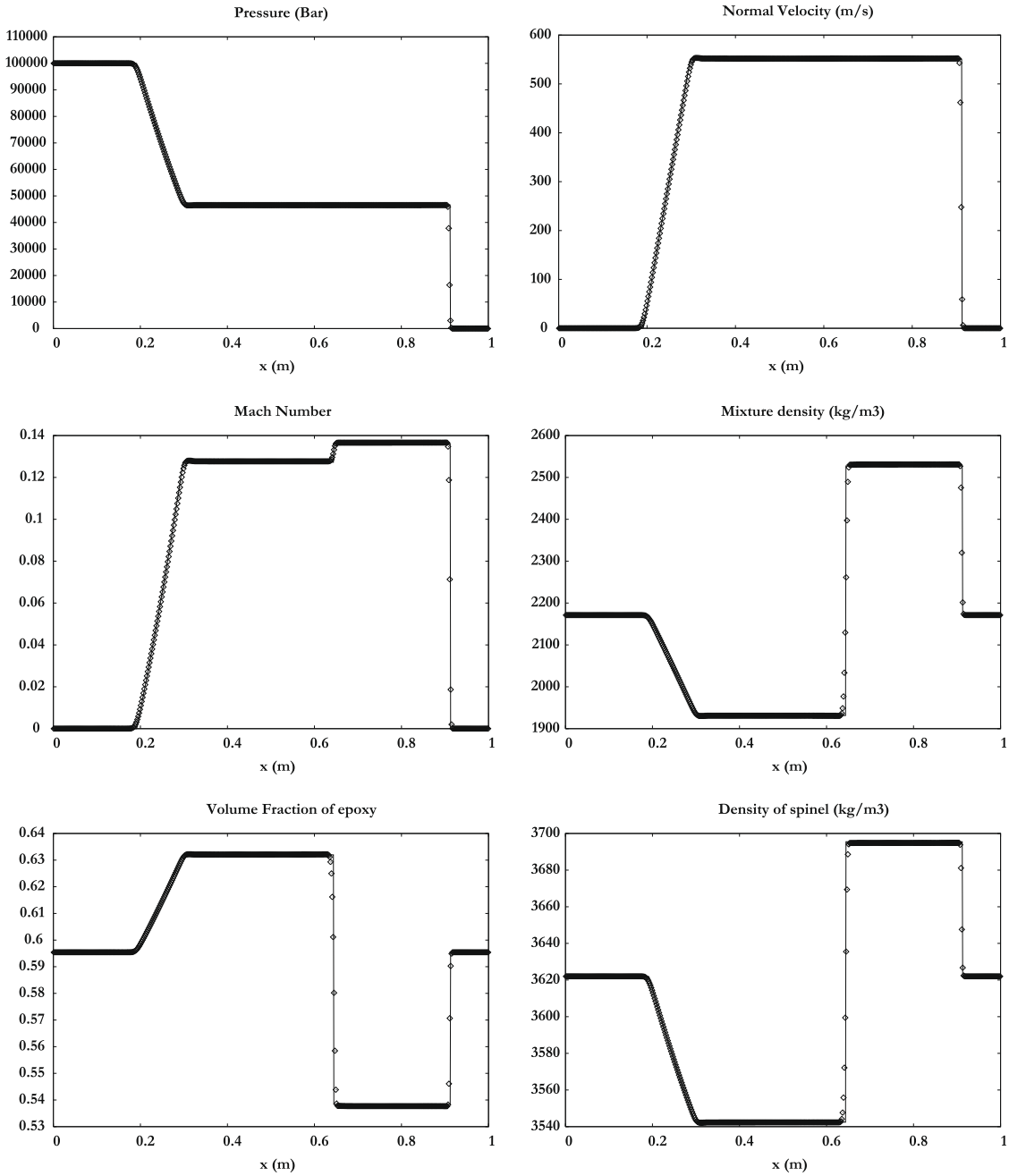

Fig. 19. Epoxy–spinel shock tube problem with moderate pressure ratio. The present relaxation method is used to solve the 6-equation model. Numerical results are shown with symbols and are compared to the exact solution of the 5-equation model (solid). A 500 cells mesh is used. The pressure ratio is 100,000 at the initial discontinuity.

shock, as shown in Fig. 18, there is no hope that this point belongs to the theoretical mixture Hugoniot curve. It follows that the corresponding volume fraction is in error. Consequently the mixture EOS (II.4) is in error too. These errors cumulate in the shock layer and, contrary to that of single phase flows, the end state does not belong to the mixture Hugoniot.

To illustrate these difficulties, consider the following test cases.

5.1. Epoxy–spinel mixture shock tube with moderate pressure ratio

A tube of 1 m length contains two chambers separated by an interface at the location $x = 0.6$ m. Both chambers of the tube are filled with the same mixture of epoxy and spinel. The initial density of the epoxy is $\rho_{epoxy} = 1185$ kg m^{-3} and its stiffened

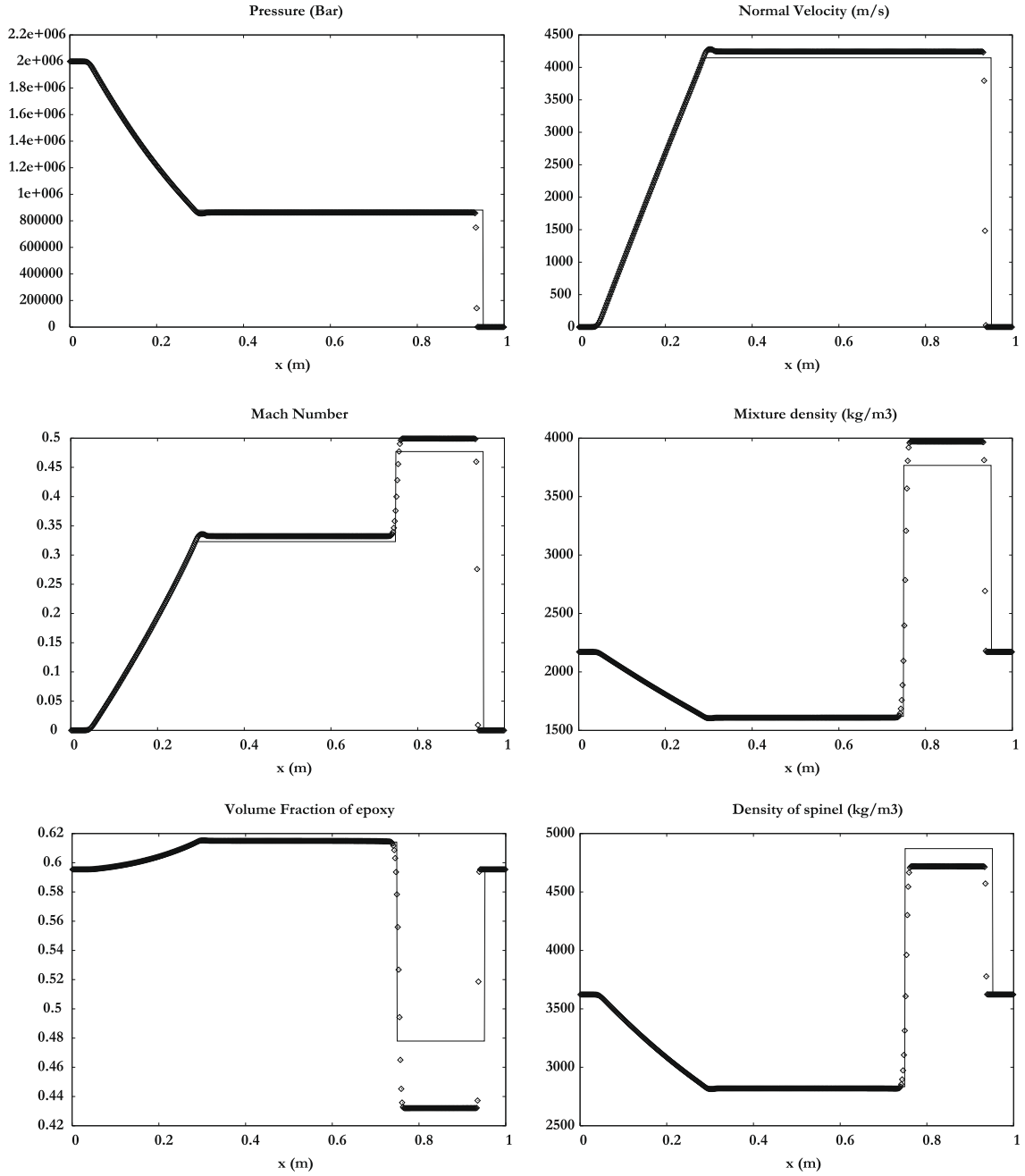

Fig. 20. Epoxy–spinel shock tube problem with extreme pressure ratio. The present relaxation method is used to solve the 6-equation model. Numerical results are shown with symbols and are compared to the exact solution of the 5-equation model (solid). A 500 cells mesh is used. The pressure ratio is 2,000,000 at the initial discontinuity.

gas EOS parameters are $\gamma_{\text{epoxy}} = 2.43$ and $p_{\infty,\text{ epoxy}} = 5.3 \times 10^9$ Pa. The initial density of spinel is $\rho_{\text{spinel}} = 3622$ kg m^{-3} and EOS parameters are $\gamma_{\text{spinel}} = 1.62$ and $p_{\infty,\text{spinel}} = 141 \times 10^9$ Pa. The initial volume fraction in both chambers are $\alpha_{\text{epoxy}} = 0.5954 (\alpha_{\text{spinel}} = 1 - \alpha_{\text{epoxy}})$. The pressure at the left of the interface is equal to 1×10^{10} Pa, while the right chamber is at atmospheric pressure. All the materials are initially at rest. Using a 500 cell uniform mesh the solution of the multiphase flow model with 6 equations is compared to the exact solution of the 5-equation model [37] in Fig. 19 at time $t = 80$ μs. As the shock is of moderate strength, the present method converges to the exact solution without any artificial heat exchange.

5.2. Epoxy–spinel mixture shock tube under extreme conditions

We consider now the same shock tube problem as previously, but the initial pressure ratio is set to 2×10^6. Results are shown in Fig. 20.

Important differences appear between solutions as the shock is now very strong. The numerical solution does not converge to the exact solution of the 5-equation model, equipped with the shock relations summarized in System (II.5). This is due to the incorrect partition of internal energy in the shock layer [37]. In order to partition the energies correctly, artificial heat exchanges are now introduced.

5.3. Artificial heat exchanges in the 6-equation model

The correct partition of the shock energy among the various phases can be achieved by shock tracking methods. Shock tracking methods have been intensively studied by Glimm et al. [18], LeVeque and Shyue [30], Massoni et al. [31]. Another option is to correct partition of the energies in the shock layer by introducing artificial heat transfers.

Artificial heat exchanges have been introduced in Petitpas et al. [37] in the context of a Lagrange-relaxation method. In the present Eulerian formulation they correspond to an extra pressure that appears in the internal energy equations:

$$\frac{\partial \alpha_1 \rho_1 e_1}{\partial t} + \frac{\partial \alpha_1 \rho_1 e_1 u}{\partial x} + (\alpha_1 p_1 + q)\frac{\partial u}{\partial x} = 0,$$
$$\frac{\partial \alpha_2 \rho_2 e_2}{\partial t} + \frac{\partial \alpha_2 \rho_2 e_2 u}{\partial x} + (\alpha_2 p_2 - q)\frac{\partial u}{\partial x} = 0.$$

The artificial heat exchange term $\pm q \frac{\partial u}{\partial x}$ is active only in the shock layer as it is defined by

$$q = \eta\left(\frac{\partial u}{\partial x}\right) v(v),$$

where $\eta\left(\frac{\partial u}{\partial x}\right) = \begin{cases} 1 \text{ if } \frac{\partial u}{\partial x} < 0 \\ 0 \text{ otherwise} \end{cases}$ and $v(v)$ is the heat exchange function.

It is more convenient and also accurate (regarding mesh independence of the results) to rewrite these equations into the form:

$$\frac{\partial \alpha_1 \rho_1 e_1}{\partial t} + \frac{\partial \left(\alpha_1 \rho_1 e_1 + \eta\left(\frac{\partial u}{\partial x}\right)\mu(v)\right) u}{\partial x} + \alpha_1 p_1 \frac{\partial u}{\partial x} = 0,$$
$$\frac{\partial \alpha_2 \rho_2 e_2}{\partial t} + \frac{\partial \left(\alpha_2 \rho_2 e_2 - \eta\left(\frac{\partial u}{\partial x}\right)\mu(v)\right) u}{\partial x} + \alpha_2 p_2 \frac{\partial u}{\partial x} = 0.$$

The function $\mu(v)$ also expresses heat exchange and must be predetermined for a given two-phase mixture. A method for its determination is given in [37]. An example of the effects of function $\mu(v)$ is shown in the following example.

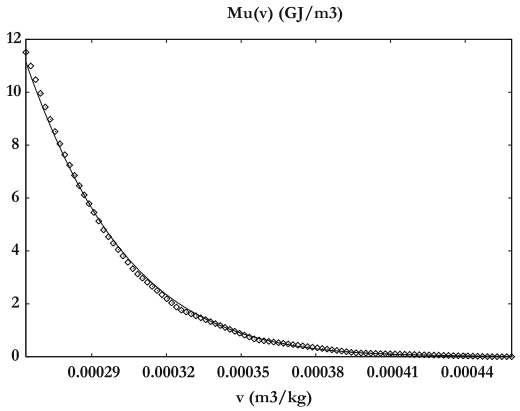

Fig. 21. Values of the approximate piecewise linear function of μ (symbols) and fitting curve ($\bar{\mu}(v) = \exp[-5.6410^7 \times v^2 + 5.3410^3 \times v + 25.6]$) in the specific volume range ($2.65 \times 10^{-4} \sim 4.61 \times 10^{-4}$ m^3/kg) corresponding to piston velocity range of $0 \sim 4200$ m/s and pressure range of 1–880,000 atm.

5.4. Epoxy–spinel mixture shock tube with artificial heat exchanges

The test problem of Fig. 20 is rerun with the artificial heat exchanges. The procedure developed in [37] is used to determine the heat exchange function. This function depends on:

- The initial state of the mixture in which the shock propagates.
- The numerical smearing of the shock front that is inherent in a given method.

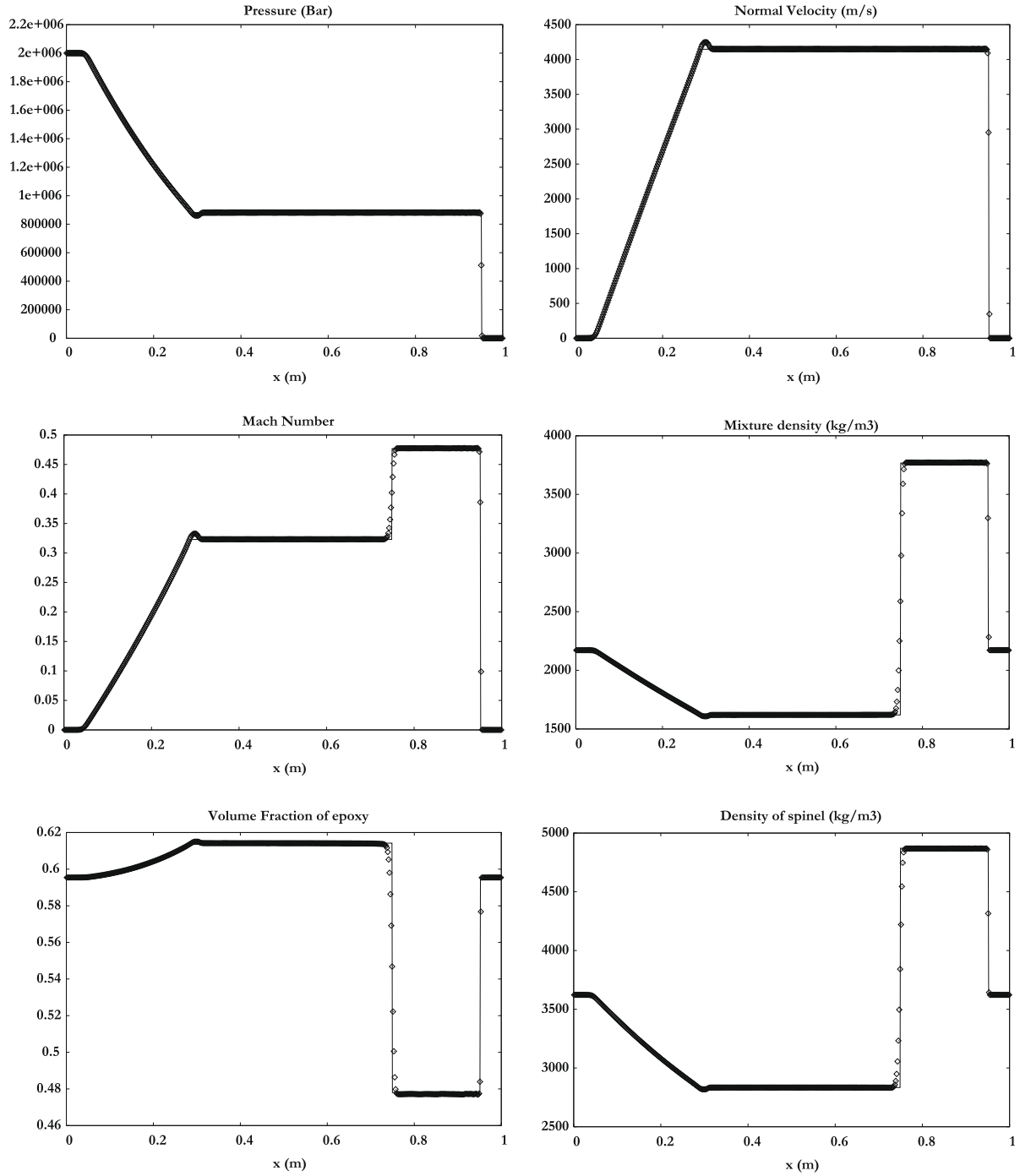

Fig. 22. Epoxy–spinel shock tube problem. The present relaxation method is used to solve the 6-equation model. Numerical results are shown with symbols and are compared to the exact solution of the 5-equation model (solid). A 500 cells mesh is used. The pressure ratio is 2,000,000 at the initial discontinuity. Artificial heat exchanges are used in the shock layer only. Convergence of the results is obtained.

For the present algorithm, the heat exchange function has been determined and is shown in Fig. 21.

Artificial heat exchanges are used in the shock layer only. With this correction, the algorithm converges to the exact solution, as shown in Fig. 22.

It is significant to note that the heat exchange function of Fig. 21 provides converged results for any shock strength in the pressure range of 1–880,000 atm. Moreover, mesh independence of the solution is guaranteed.

6. Conclusion

A relaxation hyperbolic model with 6 equations was built to solve interface problems, cavitating flows and shocks into mixtures. This model considerably simplifies the numerical approximation of the 5-equation model of Kapila et al. [23]. A simple, efficient and robust algorithm has been derived to solve the relaxation model. The various ingredients used by this method are general enough to consider future extensions to problems involving complex physics and large hyperbolic systems. In particular, solid–fluid coupling will be examined with the present multiphase modeling of diffuse interfaces in the context of the elastic model of Gavrilyuk et al. [17].

Appendix A. The link between the 6-equation model and conventional barotropic cavitating flow models

Barotropic flow models are very popular in cavitation modeling. They are composed of one or two mass conservation equations and one momentum equation. They consist in hyperbolic systems of conservation laws. These models involve an important difficulty related to the non-monotonic behavior of the sound speed versus volume fraction [26,11,48]. It is thus interesting to examine how the various ingredients developed in the context of the 6-equation model can be used for these barotropic models in order to solve this difficulty.

A well posed barotropic flow model for cavitating flows can be obtained by simplifying the 5-equation model of Kapila et al. [23]. In cavitating flows, shocks are assumed absent or weak, even if there is no evidence regarding this assumption. A first simplification consists in replacing the volume fraction and energy equations by entropy equations:

$$\begin{aligned}
&\frac{\partial s_1}{\partial t} + u\frac{\partial s_1}{\partial x} = 0,\\
&\frac{\partial s_2}{\partial t} + u\frac{\partial s_2}{\partial x} = 0,\\
&\frac{\partial (\alpha\rho)_1}{\partial t} + \frac{\partial (\alpha\rho)_1 u}{\partial x} = 0,\\
&\frac{\partial (\alpha\rho)_2}{\partial t} + \frac{\partial (\alpha\rho)_2 u}{\partial x} = 0,\\
&\frac{\partial \rho u}{\partial t} + \frac{\partial \rho u^2 + p}{\partial x} = 0.
\end{aligned} \tag{A.1}$$

This system is closed by the pressure equilibrium condition:

$$p_1(\rho_1, s_1) = p_2(\rho_2, s_2) = p. \tag{A.2}$$

Solution of this equation gives the volume fraction, and consequently the pressure p.

An extra assumption is used in conventional barotropic cavitating flow models. The entropies are assumed constant in the entire domain and not only along fluid's trajectories. The two entropy equations thus reduce to

$$s_k = s_k^0, \quad k = 1, 2.$$

The barotropic flow model thus reduces to three conservation equations:

$$\begin{aligned}
&\frac{\partial (\alpha\rho)_1}{\partial t} + \frac{\partial (\alpha\rho)_1 u}{\partial x} = 0,\\
&\frac{\partial (\alpha\rho)_2}{\partial t} + \frac{\partial (\alpha\rho)_2 u}{\partial x} = 0,\\
&\frac{\partial \rho u}{\partial t} + \frac{\partial \rho u^2 + p}{\partial x} = 0.
\end{aligned} \tag{A.3}$$

To illustrate the thermodynamic closure of this model, let us assume that each phase obeys the stiffened gas EOS (II.3). The isentropes become

$$\frac{p_k + p_{\infty k}}{\rho_k^{\gamma_k}} = \frac{p_0 + p_{\infty k}}{\rho_{0k}^{\gamma_k}},$$

and correspond to the Tait EOS.

The isentropic stiffened gas EOS (or Tait EOS), can be derived for any pure liquid and any ideal gas. It is a function of the phase density only

$$p_k = p_k^S(\rho_k) = \left(\frac{\rho_k}{\rho_{0k}}\right)^{\gamma_k}(p_0 + p_{\infty k}) - p_{\infty k}. \tag{A.4}$$

System (A.3) is thus closed by the relation

$$p_1^S(\rho_1) = p_2^S(\rho_2). \tag{A.5}$$

In other words, the mixture evolves in mechanical equilibrium with isentropic evolutions for each phase. This assumption is valid provided that boundary layers, heat and mass transfer, and shock waves have negligible influence.

With the use of the isentropic stiffened gas EOS the equilibrium condition (A.5) reduces to a function of volume fraction only:

$$f(\alpha_1) = \left(\frac{(\alpha\rho)_1}{\alpha_1\rho_{01}}\right)^{\gamma_1}(p_0 + p_{\infty 1}) - p_{\infty 1} - \left(\frac{(\alpha\rho)_2}{(1-\alpha_1)\rho_{02}}\right)^{\gamma_2}(p_0 + p_{\infty 2}) + p_{\infty 2} = 0. \tag{A.6}$$

Its resolution gives α_1, then ρ_1 as well as the pressure with the help of one of the EOS (A.4).

This model assumes that cavitation does not result from mass transfer. Cavitation pockets appear as the volume fraction increases for a small amount of gas present initially. Cavitation is thus modeled as a mechanical relaxation process, occurring at infinite rate, and not as a mass transfer process. This corresponds to a simplified limit situation compared to reality. It also presents a deficiency when pure liquid is present. Heat and mass transfers have been introduced in the 5-equation model [45] in order to deal with more realistic cavitating situations. Furthermore, the barotropic flow model, in reduced form (A.3) involves the same numerical difficulties as the 5-equation model. The sound speed for this model still obeys Wood's formulas, whose non-monotonic behavior was shown in Fig. 1.

To circumvent these difficulties, especially due to the non-monotonic behavior of the sound speed, we adapt the strategy developed in the context of the 6-equation model to this simplified situation.

A.1. A relaxation model for the barotropic cavitating flow model

The non-monotonic behavior of the sound speed that causes computational difficulties comes from the equilibrium condition (A.5). Following the analysis of Section 2, a relaxation model can be built:

$$\begin{aligned}
&\frac{\partial \alpha_1}{\partial t} + u\frac{\partial \alpha_1}{\partial x} = \mu(p_1^S(\rho_1) - p_2^S(\rho_2)),\\
&\frac{\partial (\alpha\rho)_1}{\partial t} + \frac{\partial (\alpha\rho)_1 u}{\partial x} = 0,\\
&\frac{\partial (\alpha\rho)_2}{\partial t} + \frac{\partial (\alpha\rho)_2 u}{\partial x} = 0,\\
&\frac{\partial \rho u}{\partial t} + \frac{\partial \rho u^2 + \alpha_1 p_1 + \alpha_2 p_2}{\partial x} = 0.
\end{aligned} \tag{A.7}$$

As the model includes pressure non-equilibrium effects, the momentum equation involves pressures from both phases. This model is the isentropic analogue of the 6-equation model. Unlike the preceding models, the present one has a monotonic sound speed given by

$$c_f^2 = Y_1 c_1^2 + Y_2 c_2^2.$$

It is not difficult to show that in the asymptotic limit $\mu \to +\infty$ this model corresponds to system (A.3) with thermodynamic closure (A.5).

The numerical method to solve System (A.7) is a simplification of the method developed in Section 3. It can be summarized as follows:

- At each cell boundary solve the Riemann problem of System (A.7) without relaxation terms with favorite solver. The HLLC solver of Section 3.1 is recommended.
- Evolve all flow variables $W = (\alpha_1, (\alpha\rho)_1, (\alpha\rho)_2, \rho u)$ with the Godunov type method of Section 3.2.
- Determine the relaxed pressure and especially the volume fraction by solving Eq. (A.6). The Newton method is appropriate for this task.
- Go to the first item for the next time step.

Appendix B. Asymptotic limit of the 6-equation model in the presence of stiff pressure relaxation

To perform the asymptotic analysis it is assumed that each flow variable f obeys the following asymptotic expansion: $f = f^0 + \varepsilon f^1$ where f^0 represents the equilibrium state and f^1 a small perturbation around this state. Inversely to the perturbations, pressure relaxation coefficient $\mu = \frac{\mu_0}{\varepsilon}$ is assumed stiff with $\varepsilon \to 0^+$.

With this transformation, the equations that do not contain any relaxation parameter will be unchanged. The three equations to consider are thus the internal energy equations and the volume fraction equation. These are rewritten under following form:

$$\frac{d\alpha_1}{dt} = \mu(p_1 - p_2),$$
$$\alpha_1\rho_1\frac{de_1}{dt} + \alpha_1 p_1\frac{\partial u}{\partial x} = -p_I\mu(p_1 - p_2),$$
$$\alpha_2\rho_2\frac{de_2}{dt} + \alpha_2 p_2\frac{\partial u}{\partial x} = p_I\mu(p_1 - p_2),$$

where $\frac{d}{dt} = \frac{\partial}{\partial t} + u\frac{\partial}{\partial x}$ represents the Lagrangian derivative.

Some transformations with appropriate variables are necessary before doing the asymptotic analysis. Consider the internal energy equation of phase 1. It can be written as a pressure evolution equation as $e_1 = e_1(\rho_1, p_1)$:

$$\alpha_1\rho_1\left(\left(\frac{\partial e_1}{\partial \rho_1}\right)_{p_1}\frac{d\rho_1}{dt} + \left(\frac{\partial e_1}{\partial p_1}\right)_{\rho_1}\frac{dp_1}{dt} + \frac{p_1}{\rho_1}\frac{\partial u}{\partial x}\right) = -p_I\mu(p_1 - p_2).$$

With the help of the phase 1 mass equation,

$$\frac{d\alpha_1\rho_1}{dt} + \alpha_1\rho_1\frac{\partial u}{\partial x} = 0,$$

that also reads,

$$\frac{d\rho_1}{dt} = -\frac{\rho_1}{\alpha_1}\mu(p_1 - p_2) - \rho_1\frac{\partial u}{\partial x},$$

we get

$$\frac{dp_1}{dt} + \rho_1\frac{\left(\frac{p_1}{\rho_1^2} - \frac{\partial e_1}{\partial \rho_1}\right)_{p_1}}{\left(\frac{\partial e_1}{\partial p_1}\right)_{\rho_1}}\frac{\partial u}{\partial x} = -\frac{\rho_1}{\alpha_1}\frac{\left(\frac{p_I}{\rho_1^2} - \frac{\partial e_1}{\partial \rho_1}\right)_{p_1}}{\left(\frac{\partial e_1}{\partial p_1}\right)_{\rho_1}}\mu(p_1 - p_2).$$

With the help of sound speed definitions,

$$c_1^2 = \frac{\left(\frac{p_1}{\rho_1^2} - \frac{\partial e_1}{\partial \rho_1}\right)_{p_1}}{\left(\frac{\partial e_1}{\partial p_1}\right)_{\rho_1}},$$

$$c_{I1}^2 = \frac{\left(\frac{p_I}{\rho_1^2} - \frac{\partial e_1}{\partial \rho_1}\right)_{p_1}}{\left(\frac{\partial e_1}{\partial p_1}\right)_{\rho_1}}.$$

The phase 1 pressure evolution equation is obtained:

$$\frac{dp_1}{dt} + \rho_1 c_1^2\frac{\partial u}{\partial x} = -\frac{\rho_1 c_{I1}^2}{\alpha_1}\mu(p_1 - p_2).$$

Regarding phase 2, a similar result is obtained:

$$\frac{dp_2}{dt} + \rho_2 c_2^2\frac{\partial u}{\partial x} = \frac{\rho_2 c_{I2}^2}{\alpha_2}\mu(p_1 - p_2).$$

The asymptotic analysis is now carried out on the following system:

$$\frac{d\alpha_1}{dt} = \mu(p_1 - p_2),$$
$$\frac{dp_1}{dt} + \rho_1 c_1^2\frac{\partial u}{\partial x} = -\frac{\rho_1 c_{I1}^2}{\alpha_1}\mu(p_1 - p_2),$$
$$\frac{dp_2}{dt} + \rho_2 c_2^2\frac{\partial u}{\partial x} = \frac{\rho_2 c_{I2}^2}{\alpha_2}\mu(p_1 - p_2).$$

By expanding each flow variable as $f = f^0 + \varepsilon f^1$ we get

– At order $\frac{1}{\varepsilon}$:

$$p_1^0 = p_2^0 = p^0.$$

It implies on the one hand,

$$p_I^0 = p^0,$$

and on the other hand:

$$c_{I1}^{0^2} = c_1^{0^2} \quad \text{and} \quad c_{I2}^{0^2} = c_2^{0^2}.$$

– At zero-order the two-pressure equations become

$$\frac{dp^0}{dt} + \rho_1^0 c_1^{0^2} \frac{\partial u^0}{\partial x} = -\frac{\rho_1^0 c_1^{0^2}}{\alpha_1^0}(p_1^1 - p_2^1),$$
$$\frac{dp^0}{dt} + \rho_2^0 c_2^{0^2} \frac{\partial u^0}{\partial x} = \frac{\rho_2^0 c_2^{0^2}}{\alpha_2^0}(p_1^1 - p_2^1).$$

By making the difference of these two equations, the pressure fluctuation difference is readily obtained:

$$p_1^1 - p_2^1 = \frac{\rho_2^0 c_2^{0^2} - \rho_1^0 c_1^{0^2}}{\frac{\rho_1^0 c_1^{0^2}}{\alpha_1^0} + \frac{\rho_2^0 c_2^{0^0}}{\alpha_2^0}} \frac{\partial u^0}{\partial x}.$$

The volume fraction equation thus becomes

$$\frac{d\alpha_1^0}{dt} = \frac{\rho_2^0 c_2^{0^2} - \rho_1^0 c_1^{0^2}}{\frac{\rho_1^0 c_1^{0^2}}{\alpha_1^0} + \frac{\rho_2^0 c_2^{0^0}}{\alpha_2^0}} \frac{\partial u^0}{\partial x}.$$

Consequently the 5-equation model with mechanical equilibrium is recovered as the asymptotic limit of the 6-equation model in the presence of stiff pressure relaxation.

Appendix C. Extension to second-order

The first-order numerical method for the hyperbolic step presented in Section 3 is extended to second-order. It consists in solving the two-pressure 6-equation model (C.1) with a MUSCL type method:

$$\begin{aligned}
&\frac{\partial \alpha_1}{\partial t} + u\frac{\partial \alpha_1}{\partial x} = 0,\\
&\frac{\partial \alpha_1\rho_1}{\partial t} + \frac{\partial \alpha_1\rho_1 u}{\partial x} = 0,\\
&\frac{\partial \alpha_2\rho_2}{\partial t} + \frac{\partial \alpha_2\rho_2 u}{\partial x} = 0,\\
&\frac{\partial \rho u}{\partial t} + \frac{\partial \rho u^2 + (\alpha_1 p_1 + \alpha_2 p_2)}{\partial x} = 0,\\
&\frac{\partial \alpha_1\rho_1 e_1}{\partial t} + \frac{\partial \alpha_1\rho_1 e_1 u}{\partial x} + \alpha_1 p_1 \frac{\partial u}{\partial x} = 0,\\
&\frac{\partial \alpha_2\rho_2 e_2}{\partial t} + \frac{\partial \alpha_2\rho_2 e_2 u}{\partial x} + \alpha_2 p_2 \frac{\partial u}{\partial x} = 0.
\end{aligned} \tag{C.1}$$

In the MUSCL method, the solution is assumed regular enough so that a primitive variable formulation can be used:

$$\begin{aligned}
&\frac{\partial \alpha_1}{\partial t} + u\frac{\partial \alpha_1}{\partial x} = 0,\\
&\frac{\partial \rho_1}{\partial t} + u\frac{\partial \rho_1}{\partial x} + \rho_1\frac{\partial u}{\partial x} = 0,\\
&\frac{\partial \rho_2}{\partial t} + u\frac{\partial \rho_2}{\partial x} + \rho_2\frac{\partial u}{\partial x} = 0,\\
&\frac{\partial u}{\partial t} + u\frac{\partial u}{\partial x} + \frac{1}{\rho}\frac{\partial p}{\partial x} = 0 \quad \text{or} \quad \frac{\partial u}{\partial t} + u\frac{\partial u}{\partial x} + \frac{p_1 - p_2}{\rho}\frac{\partial \alpha_1}{\partial x} + \frac{\alpha_1}{\rho}\frac{\partial p_1}{\partial x} + \frac{(1-\alpha_1)}{\rho}\frac{\partial p_2}{\partial x} = 0,\\
&\frac{\partial p_1}{\partial t} + u\frac{\partial p_1}{\partial x} + \rho_1 c_1^2\frac{\partial u}{\partial x} = 0,\\
&\frac{\partial p_2}{\partial t} + u\frac{\partial p_2}{\partial x} + \rho_2 c_2^2\frac{\partial u}{\partial x} = 0.
\end{aligned}$$

Under compact form, this system reads

$$\frac{\partial W}{\partial t} + A(W)\frac{\partial W}{\partial x} = 0. \tag{C.2}$$

With $W = (\alpha_1,\rho_1,\rho_2,u,p_1,p_2)^t$ and $A(W) = \begin{pmatrix} u & 0 & 0 & 0 & 0 & 0 \\ 0 & u & 0 & \rho_1 & 0 & 0 \\ 0 & 0 & u & \rho_2 & 0 & 0 \\ \frac{p_1-p_2}{\rho} & 0 & 0 & u & \frac{\alpha_1}{\rho} & \frac{1-\alpha_1}{\rho} \\ 0 & 0 & 0 & \rho_1 c_1^2 & u & 0 \\ 0 & 0 & 0 & \rho_2 c_2^2 & 0 & u \end{pmatrix}$.

Second-order extension consists in applying the following sequence of operations.

C.1. Gradients limitation

In a cell i, at instant t^n, primitive variables W_i^n are known. Let us denote by Δ_i^- and Δ_i^+ the gradients vector respectively on the left and right neighbors of cell i. They are defined by

$$\Delta_i^- = \frac{W_i^n - W_{i-1}^n}{\Delta x} \quad \text{and} \quad \Delta_i^+ = \frac{W_{i+1}^n - W_i^n}{\Delta x}.$$

A slope limiter function ξ is used to prevent local extrema. Minmod, van Leer or Superbee limiters can be used. The limited slope is now $\Delta_i = \xi(\Delta_i^-, \Delta_i^+)$.

C.2. Variables extrapolation

Within a given cell extrapolated primitive variable vectors $W_{i,L}$ and $W_{i,R}$ corresponding to the left and right boundary of cell i respectively are computed,

$$W_{i,L}^n = W_i^n - \frac{\Delta x}{2}\Delta_i \quad \text{and} \quad W_{i,R}^n = W_i^n + \frac{\Delta x}{2}\Delta_i.$$

These variables are evolved during a half time step by

$$W_{i,L,R}^{n+1/2} = W_{i,L,R}^n + \frac{1}{2}\frac{\Delta t}{\Delta x}A(W_i^n)\left[W_{i,L}^n - W_{i,R}^n\right].$$

C.3. Riemann problem resolutions

The Riemann problem is now computed at each cell boundary $i \pm 1/2$ allowing flux vectors $F_{i\pm1/2}^*$ computation for conservative variables:

$$F_{i-1/2}^* = F_{i-1/2}^*\left(W_{i-1,R}^{n+1/2}; W_{i,L}^{n+1/2}\right) \quad \text{and} \quad F_{i+1/2}^* = F_{i+1/2}^*\left(W_{i,R}^{n+1/2}; W_{i+1,L}^{n+1/2}\right). \tag{C.3}$$

It also provides the cell boundaries non-conservative variables:

$$\alpha_{k,i\pm1/2}^*, u_{i\pm1/2}^* \quad \text{and} \quad (\alpha\rho e)_{k,i\pm1/2}^*. \tag{C.4}$$

C.4. Evolution step

Once the inter-cells fluxes and non-conservative variables are determined, the solution is evolved on the entire time step:

$$U_i^{n+1} = U_i^n - \frac{\Delta t}{\Delta x}(F_{i+1/2}^* - F_{i-1/2}^*),$$
$$\alpha_{1i}^{n+1} = \alpha_{1i^n} - \frac{\Delta t}{\Delta x}((u\alpha_1)_{i+1/2}^* - (u\alpha_1)_{i-1/2}^* - \alpha_1 i^n(u_{i+1/2}^* - u_{i-1/2}^*)),$$
$$(\alpha\rho e)_k i^{n+1} = (\alpha\rho e)_{ki}^n - \frac{\Delta t}{\Delta x}((\alpha\rho e u)_{ki+1/2}^* - (\alpha\rho e u)_{ki-1/2}^* + (\alpha p)_{ki}^n(u_{i+1/2}^* - u_{i-1/2}^*)),$$

where the "*" variables are given by (C.3) and (C.4).

Appendix D. Extension to multi-dimensions

The method is extended to multi-dimensions by a finite volume method able to deal with structured and unstructured meshes. Thus, let us consider a control volume V_i delimited by surface A of normal unit vector $\vec{n}$. The conservative part of system (III.1) under integral form reads

$$\frac{\partial}{\partial t}\int_{V_i} U + \int_A H \bullet \vec{n} dA = 0 \tag{D.1}$$

with $U = ((\alpha\rho)_1,(\alpha\rho)_2,\rho u,\rho v,\rho E)^T$ the conservative variable vector,

H = (*F*,*G*) the tensor of fluxes where:

$$F = ((\alpha\rho)_1 u, (\alpha\rho)_1 u, \rho u^2 + p, uv, (\rho E + p)u)^{\mathrm{T}},$$
$$G = ((\alpha\rho)_1 v, (\alpha\rho)_1 v, \rho uv, \rho v^2 + p, (\rho E + p)v)^{\mathrm{T}},$$

and $E = Y_1 e_1 + Y_2 e_2 + \frac{1}{2}u^2 + \frac{1}{2}v^2$ and $p = \alpha_1 p_1 + \alpha_2 p_2$.

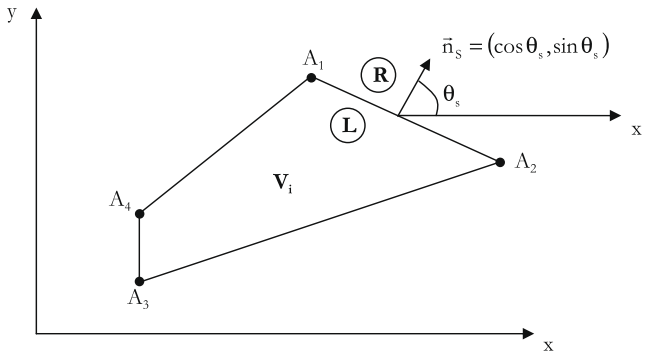

Boundary A of V_i is the union of N straight segments $[A_sA_{s+1}]$, where $A_{N+1} = A_1$.

The first term of Eq. (D.1) is interpreted as the time-rate of change of the conservative variable vector volume average:

$$\frac{\partial}{\partial t}\int_{V_i} U = V_i \frac{\partial \overline{U}}{\partial t}.$$

As the normal unit vector is expressed by $\vec{n}_S = (\cos\theta_s, \sin\theta_s)$, the second term of (D.1) becomes

$$\int_A \mathbf{H} \bullet \vec{n} dA = \sum_{s=1}^{N} \int_{A_s}^{A_{s+1}} \mathbf{H} \bullet \vec{n}_S dA = \sum_{s=1}^{N} \int_{A_s}^{A_{s+1}} (F \cdot \cos\theta_s + G \cdot \sin\theta_s) dA.$$

Assuming that the fluxes are constant along each segment, it becomes

$$\int_A \mathbf{H} \bullet \vec{n} dA = \sum_{s=1}^{N} L_s (F_s \cdot \cos\theta_s + G_s \cdot \sin\theta_s),$$

where L_s is the length of segment $[A_sA_{s+1}]$.

After time integration, the evolution of the conservative part of system (III.1) is given for cell *i* by the scheme:

$$U_i^{n+1} = U_i^n - \frac{\Delta t}{V_i}\sum_{s=1}^{N} L_s (F_s^* \cdot \cos\theta_s + G_s^* \cdot \sin\theta_s),$$

where F_s^* and G_s^* represent the fluxes solution of the Riemann problem between states *L* and *R* separated by the segment $[A_sA_{s+1}]$ with respect to normal $\vec{n}$.

The scheme for the non-conservative volume fraction equation becomes

$$\alpha_{k,i}^{n+1} = \alpha_{k,i}^n - \frac{\Delta t}{V_i}\sum_{s=1}^{N} L_s [(u\alpha_k)_s^* \cos\theta_s + (v\alpha_k)_s^* \sin\theta_s - \alpha_{k,i}^n (u_s^* \cos\theta_s + v_s^* \sin\theta_s)],$$

and for the non-conservative energy equations it is

$$(\alpha\rho e)_{k,i}^{n+1} = (\alpha\rho e)_{k,i}^n - \frac{\Delta t}{V_i}\sum_{s=1}^{N} L_s [((\alpha\rho e)_k u)_s^* \cos\theta_s + ((\alpha\rho e)_k v)_s^* \sin\theta_s + (\alpha p)_{k,i}^n (u_s^* \cos\theta_s + v_s^* \sin\theta_s)].$$

References

[1] R. Abgrall, How to prevent pressure oscillations in multicomponent flow calculations: a quasi conservative approach, Journal of Computational Physics 125 (1996) 150–160.
[2] R. Abgrall, S. Karni, Computations of compressible multifluids, Journal of Computational Physics 169 (2) (2001) 594–623.
[3] R. Abgrall, V. Perrier, Asymptotic expansion of a multiscale numerical scheme for compressible multiphase flows, SIAM Journal of Multiscale and Modeling and Simulation 5 (2006) 84–115.
[4] R. Abgrall, R. Saurel, Discrete equations for physical and numerical compressible multiphase mixtures, Journal of Computational Physics 186 (2) (2003) 361–396.
[5] M.R. Baer, J.W. Nunziato, A two-phase mixture theory for the deflagration-to-detonation transition (DDT) in reactive granular materials, International Journal of Multiphase Flow 12 (6) (1986) 861.

[6] J.B. Bdzil, R. Menikoff, S.F. Son, A.K. Kapila, D.S. Steward, Two-phase modeling of a deflagration-to detonation transition in granular materials: A critical exmination of modeling issues, Physics of Fluids 11 (2) (1999) 378–402.
[7] D.J. Benson, Computational methods in Lagrangian and Eulerian hydrocodes, Computer Methods in Applied Mechanics and Engineering 99 (1992) 235–394.
[8] A. Chinnayya, E. Daniel, R. Saurel, Computation of detonation waves in heterogeneous energetic materials, Journal of Computational Physics 196 (2004) 490–538.
[9] G. Cochran, J. Chan, Shock initiation and detonation models in one and two dimensions, CID-18024 Lawrence National Laboratory Report 2 (1979) 1–2.
[10] R. Courant, K. Friedrichs, Supersonic Flow and Shock Waves, Springer, 1948.
[11] O. Coutier-Delgosha, R. Fortes-Patella, J.L. Reboud, N. Hakimi, C. Hirsch, Stability of preconditioned Navier-Stockes equations associated with a cavitation model, Computers and Fluids 34 (2005) 319–349.
[12] S.F. Davis, Simplified second order Godunov type methods, SIAM Journal of Scientific and Statistical Computing 9 (1988) 445–473.
[13] A. Dervieux, F. Thomasset, A finite element method for the simulation of Rayleigh-Taylor instability, in: Approximation methods for Navier–Stokes problems, Proceedings of the Symposium, Paderborn, West Germany, September 9–15, 1979, Springer-Verlag, Berlin, 1980, pp. 145–158.
[14] C. Farhat, F.X. Roux, A method for finite element tearing and interconnecting and its parallel solution algorithm, International Journal for Numerical Methods in Engineering 32 (1991) 1205–1227.
[15] N. Favrie, S. Gavrilyuk, R. Saurel, Diffuse solid–fluid interface model in cases of extreme deformations, Journal of Computational Physics, submitted for publication.
[16] R. Fedkiw, T. Aslam, B. Merriman, S. Osher, A non-oscillatory Eulerian approach to interfaces in multimaterial flows (the ghost fluid method), Journal of Computational Physics 152 (2) (1999) 457–492.
[17] S. Gavrilyuk, N. Favrie, R. Saurel, Modelling wave dynamics of compressible elastic materials, Journal of Computational Physics 227 (5) (2008) 2941–2969.
[18] J. Glimm, J.W. Grove, X.L. Li, K.M. Shyue, Q. Zhang, Y. Zeng, Three dimensional front tracking, SIAM Journal of Scientific Computing 19 (1998) 703–727.
[19] D. Gueyffier, L. Li, A. Nadim, R. Scardovelli, S. Zaleski, Volume-of-fluid interface tracking with smoothed surface stress methods for three-dimensional flows, Journal of Computational Physics 152 (1999) 423–456.
[20] C.W. Hirt, B.D. Nichols, Volume of fluid (VOF) method for the dynamics of free boundaries, Journal of Computational Physics 39 (1981) 201–255.
[21] C.W. Hirt, A.A. Amsden, J.L. Cook, An arbitrary Lagrangian Eulerian computing method for all flow speeds, Journal of Computational Physics 135 (1974) 203–216.
[22] T.Y. Hou, P. Le Floch, Why non-conservative schemes converge to the wrong solution: error analysis, Mathematics of Computation 62 (1994) 497–530.
[23] A.K. Kapila, R. Menikoff, J.B. Bdzil, S.F. Son, D.S. Stewart, Two-phase modeling of deflagration-to-detonation transition in granular materials: reduced equations, Physics of Fluids 13 (10) (2001) 3002–3024.
[24] S. Karni, Multicomponent flow calculations by a consistent primitive algorithm, Journal of Computational Physics 112 (1994) 31–43.
[25] B.C. Khoo, T.G. Liu, C.W. Wang, The ghost fluid method for compressible gas-water simulations, Journal of Computational Physics 204 (2005) 193.
[26] B. Koren, M.R. Lewis, E.H. van Brummelen, B. van Leer, Riemann-problem and level-set approaches for homentropic two-fluid computations, Journal of Computational Physics 181 (2002) 654–674.
[27] G. Layes, O. Le Métayer, Quantitative numerical and experimental studies of the shock accelerated heterogeneous bubbles motion, Physics of Fluids 19 (2007) 042105.
[28] E.L. Lee, H.C. Horning, J.W. Kury, Adiabatic Expansion of High Explosives Detonation Products, Lawrence Radiation Laboratory, University of California, Livermore, TID 4500-UCRL 50422, 1968.
[29] O. Le Metayer, J. Massoni, R. Saurel, Modeling evaporation fronts with reactive Riemann solvers, Journal of Computational Physics 205 (2005) 567–610.
[30] R.J. LeVeque, Keh-Ming Shyue, Two-dimensional front tracking based on high resolution wave propagation methods, Journal of Computational Physics 123 (2) (1996) 354–368.
[31] J. Massoni, R. Saurel, G. Baudin, G. Demol, A mechanistic model for shock initiation of solid explosives, Physics of Fluids 11 (3) (1999) 710–736.
[32] G.H. Miller, E.G. Puckett, A high-order Godunov method for multiple condensed phases, Journal of Computational Physics 128 (1) (1996) 134–164.
[33] G.H. Miller, P. Colella, A high-order Eulerian Godunov method for elastic–plastic flows in solids, Journal of Computational Physics 167 (2001) 131–176.
[34] W. Mulder, S. Osher, J.A. Sethian, Computing interface motion: the compressible Rayleigh-Taylor and Kelvin-Helmholtz instabilities, Journal of Computational Physics 100 (1992) 209.
[35] A. Murrone, H. Guillard, A five equation reduced model for compressible two phase flow problems, Journal of Computational Physics 202 (2) (2005) 664–698.
[36] S. Osher, R. Fedkiw, Level set methods: an overview and some recent results, Journal of Computational Physics 169 (2001) 463–502.
[37] F. Petitpas, E. Franquet, R. Saurel, O. Le Metayer, A relaxation-projection method for compressible flows. Part II. The artificial heat exchange for multiphase shocks, Journal of Computational Physics 225 (2) (2007) 2214–2248.
[38] F. Petitpas, R. Saurel, E. Franquet, A. Chinnayya, A., Modelling detonation waves in condensed materials: multiphase CJ conditions and multidimensional computations, Shock waves, submitted for publication.
[39] G. Perigaud, R. Saurel, A compressible flow model with capillary effects, Journal of Computational Physics 209 (2005) 139–178.
[40] R. Saurel, R. Abgrall, A multiphase Godunov method for multifluid and multiphase flows, Journal of Computational Physics 150 (1999) 425–467.
[41] R. Saurel, O. Le Metayer, A multiphase model for interfaces, shocks, detonation waves and cavitation, Journal of Fluid Mechanics 431 (2001) 239–271.
[42] R. Saurel, S. Gavrilyuk, F. Renaud, A multiphase model with internal degrees of freedom: application to shock-bubble interaction, Journal of Fluid Mechanics 495 (2003) 283–321.
[43] R. Saurel, E. Franquet, E. Daniel, O. Le Metayer, A relaxation-projection method for compressible flows. Part I. The numerical equation of state for the Euler equations, Journal of Computational Physics 223 (2) (2007) 822–845.
[44] R. Saurel, O. Le Metayer, J. Massoni, S. Gavrilyuk, Shock jump relations for multiphase mixtures with stiff mechanical relaxation, Shock Waves 16 (3) (2007) 209–232.
[45] R. Saurel, F. Petitpas, R. Abgrall, Modeling phase transition in metastable liquids. Application to cavitating and flashing flows, Journal of Fluid Mechanics 607 (2008) 313–350.
[46] D.R. Scheffer, J.A. Zukas, Practical aspects of numerical simulation of dynamic events: material interfaces, International Journal of Impact Engineering 24 (5–6) (2000) 821–842.
[47] J. Sethian, Evolution, implementation and application of level set and fast marching methods for advancing fronts, Journal of Computational Physics 169 (2001) 503–555.
[48] E. Sinibaldi, Implicit preconditioned numerical schemes for the simulation of three-dimensional barotropic flows, PhD Thesis, Scuola Normale Superiore di Pisa, Italy, 2006.
[49] H.B. Stewart, B. Wendroff, Two-phase flow: models and methods, Journal of Computational Physics 56 (3) (1984) 363–409.
[50] V.A. Titarev, E. Romenski, E.F. Toro, MUSTA type upwind fluxes for nonlinear elasticity, International Journal of Numerical Methods in Engineering 73 (7) (2007) 897–926.
[51] E.F. Toro, M. Spruce, W. Speares, Restoration of the contact surface in the HLL Riemann solver, Shock Waves 4 (1994) 25–34.
[52] E.F. Toro, Riemann Solvers and Numerical Methods for Fluids Dynamics, Springer-Verlag, Berlin, 1997.
[53] E.H. van Brummelen, B. Koren, A pressure-invariant conservative Godunov-type method for barotropic two-fluid flows, Journal of Computational Physics 185 (2003) 289–308.
[54] A.B. Wood, A Textbook of Sound, G. Bell and Sons Ltd., London, 1930.